FINAL TECHNICAL REPORT

Grant No. DE-SC0013720 Grantee: University of Miami
Period of Performance: 06/01/15- 05/31/18

Project Title: Support for the Planning of the Layered Atlantic Smoke Interactions with Clouds (LASIC) AMF1 Deployment

Paquita Zuidema, PI-UM

Paquita Zuidema, University of Miami
Matthew Alvarado, Atmospheric and Environmental Research
Christine Chiu, Colorado State University
Simon DeSzoeke, Oregon State University
Chris Fairall, University of Colorado
Graham Feingold, NOAA Earth Systems Resources Laboratory
Andrew Freedman, Aerodyne
Steve Ghan, Pacific Northwest National Laboratory
James Haywood, University of Exeter
Pavlos Kollias, McGill University
Ernie Lewis, Brookhaven National Laboratory
Greg McFarquhar, Oklahoma University
Allison McComiskey, University of Colorado
David Mechem, University of Kansas
Tim Onasch, Aerodyne
Jens Redemann, NASA Ames
David Romps, Lawrence Berkeley Laboratory
David Turner, National Severe Storms Laboratory
Hailong Wang, Pacific Northwest National Laboratory
Robert Wood, University of Washington
Sandra Yuter, North Carolina State University
Ping Zhu, Florida International University

April 2018

Work supported by the U.S. Department of Energy,
Office of Science, Office of Biological and Environmental Research

Executive Summary

Southern Africa is the world's largest emitter of biomass burning aerosols. Their westward transport over the remote southeast Atlantic ocean colocates some of the largest atmospheric loadings of absorbing aerosol with the least examined of the Earth's major subtropical stratocumulus decks. Global aerosol model results highlight that the largest positive top-of-atmosphere forcing in the world occurs in the southeast Atlantic, but this region exhibits large differences in magnitude and sign between reputable models, in part because of high variability in the underlying model cloud distributions. Many uncertainties contribute to the highly variable model radiation fields: the aging of the shortwave-absorbing aerosol during transport, how much of the aerosol mixes into the cloudy boundary layer, and how the low clouds adjust to smoke-radiation and smoke-cloud interactions. In addition, the ability of the biomass burning aerosol to absorb shortwave radiation is known to vary seasonally as the fuel type on land changes. LASIC (Layered Atlantic Smoke Interactions with Clouds) is a strategy to improve our understanding of aged carbonaceous aerosol, its seasonal evolution, and the mechanisms by which clouds adjust to the presence of the aerosol. The observational strategy centers on deploying the AMF1 cloud, aerosol, and atmospheric profiling instrumentation to Ascension Island, located within the trade-wind shallow cumulus regime (14.5^{o}W, 8^{o}S) 3000 km offshore of continental Africa. The location is within the latitude zone of the maximum outflow of aerosol, with the deepening boundary layer known to entrain free-tropospheric smoke. The primary activities for LASIC are: 1) to improve current knowledge on aged biomass burning aerosol and its radiative properties as a function of the seasonal cycle; 2) to use surface-based remote sensing to sensitively interrogate the atmosphere for the relative vertical location of aerosol and clouds; 3) to improve our understanding of the cloud adjustments to the presence of shortwave-absorbing aerosol within the vertical column, both through aerosol-radiation and through aerosol-cloud interactions; 4) to aid low cloud parameterization efforts for climate models. The measurements span June 1, 2016 - October 31, 2017, encompassing two July-October biomass burning seasons. The August-September, 2016, months include an Intensive Observing Period (IOP) with 8x/daily radiosondes. In 2017, from 16 August through 7 September, the UK FAAM Bae-146 plane was deployed from Ascension, providing complementary data on the atmosphere's vertical structure as part of the CLARIFY project, with similar scientific goals. The NASA ORACLES aircraft campaign, sharing similar objectives to LASIC, deployed from Namibia in September, 2016, and Sao Tome in August, 2017. The latter included a suitcase flight to Ascension spanning August 18-21. In 2017 a CAPS-SSA instrument belonging to Aerodyne was brought to Ascension, gathering data primarily for August, towards providing a second, independent measurement of aerosol absorption. Ascension Island is also an AERONET site.

Acronyms and Abbreviations

Create a list of acronyms, if any were used in the report.

ABE	Aerosol Best Estimate
ACSM	Aerosol Chemistry Speciation Monitor
AEROCOM	Aerosol Comparisons between Observations and Models – an international aerosol modeling intercomparison initiative focused on understanding global aerosol and its impact on climate
AMF	ARM Mobile Facility
AMF1	first ARM Mobile Facility
AERONET	Aerosol Robotic Network
AMSR-E	Advanced Microwave Scanning Radiometer-E
AOD	aerosol optical depth
ARM	Atmospheric Radiation Measurement
ARSCL	Active Remote Sensing of Cloud Locations
BB	biomass burning
BBC	British Broadcasting Corporation
BC	black carbon
CALIOP	Cloud Aerosol Lidar with Orthogonal Polarization
CAM5	Community Atmosphere Model version 5
CAP-MBL	Clouds, Aerosols, Precipitation in the Marine Boundary Layer
CCN	cloud condensation nuclei
CERES	Clouds and Earths' Radiant System
CESM	Community Earth System Model
CLARIFY	Cloud-Aerosol-Radiation Interactions and Forcing
CloudSat	a NASA satellite that studies the role of clouds and aerosols in regulating Earth's weather, climate, and air quality

CMIP	Coupled Model Intercomparison Project – a standard experimental protocol for studying the output of coupled atmosphere-ocean general circulation models
DOE	U. S. Department of Energy
ERA	European Reanalysis of the Global Climate System – an atmospheric reanalysis of the 20th century developed by the European Centre for Medium-Range Weather Forecasts
FLEXPART-WRF	FLEXible PARTicle dispersion model – a combination of Weather Research and Forecasting meteorological fields with a Lagrangian particle dispersion model
GNDRAD	Ground Radiation – an ARM collection of radiometers that provides continuous measurements of broadband shortwave (solar) and longwave (infrared) irraiances for upwelling atmospheric components
GPCI	GEWEX/WGNE Pacific Cross-section Intercomparison – a Global Energy and Water Cycle Experiment/Working Group for Numerical Experimentation program to evaluate climate and weather prediction models in the tropics and sub-tropics, using satellite observations
HSRL	high-spectral-resolution lidar
HYSPLIT	Hybrid Single Particle Lagrangian Integrated Trajectory Model – a NOAA Air Resources Laboratory system for computing simple air parcel trajectories to complex dispersion and deposition simulations
INDOEX	Indian Ocean Experiment – an NCAR field study of the role of anthropogenic aerosols in climate change that was conducted from January through March 1999 over the tropical Indian Ocean
IOP	intensive observational period
KASACR	K-Band Scanning Cloud Radar
Ka/W-SACR	Ka/W-Scanning ARM Cloud Radars
LASIC	Layered Atlantic Smoke Interactions with Clouds
LBLRTM	Line-By-Line Radiative Transfer Model
LES	large-eddy simulation
LWP	liquid water path
MAM	modal aerosol module developed for the CAM5
MAOS	Mobile Aerosol Observing System

MAOS-A	MAOS-Aerosol
MAOS-C	MAOS-Chemistry
MFRSR	Multifilter Rotating Shadowband Radiometer
MMF	multi-scale modeling framework
MODIS	Moderate Resolution Imaging Spectroradiometer
MPL	micropulse lidar
MPLNET	Micro-Pulse Lidar Network – a NASA network of MPL systems that measures aerosol and cloud vertical structure continuously, day and night, over long periods
MWRHF	Microwave Radiometer, High Frequency
MWR3C	Microwave Radiometer, 3-Channel
NASA	National Aeronautics and Space Administration
NASA-ORACLES	National Aeronautics and Space Administration Observations of Aerosols above Clouds and their Interactions
NCAR	National Center for Atmospheric Research
NFOV	Narrow Field of View – an ARM instrument
NIR	near-infrared regions
NOAA	National Oceanic and Atmospheric Administration
PASS	Photo-Acoustic Soot Spectrometer
PCASP	Passive Cavity Aerosol Spectrometer Probe
PI	principal investigator
PNNL	Pacific Northwest National Laboratory
POM	particulate organic matter
POP	precipitation of probability
PSAP	Particle Soot Absorption Photometer
RICO	Rain In Cumulous over the Ocean

RIPBE	Radiatively Important Parameters Best Estimate
RWP	Radar Wind Profiler
SAFARI-UK	Southern African Regional science Initiative
SAS-He	Solar Array Spectrometer – Hemispheric
SAS-Ze	Solar Array Spectrometer – Zenith
SCM	single-column model
SEBS	surface energy balance system
SKYRAD	Sky Radiation – an ARM collection of radiometers providing continuous measurements of broadband shortwave (solar), longwave (infrared), and ultraviolet irradiances for downwelling atmospheric components
SMPS	Scanning Mobility Particle Sizer
SPOP	susceptibility of POP
SSA	single-scattering albedo
SST	sea surface temperature
UHSAS	Ultra-High-Sensitivity Aerosol Spectrometer
UK	United Kingdom
US	United States
VAMOS	Variability of the American Monsoon System
VAPs	value-added products
VARANAL	Constrained Variational Analysis – an ARM value-added proudct
VBS	Volatility Basis Set
VOCALS	VAMOS Ocean-Cloud-Atmosphere-Land Study
WACR	W-Band Zenith Cloud Radar
WRF	Weather Research and Forecasting Model
WRF-Chem	Weather Research and Forecasting Model coupled with Chemistry
WSACR	W-Band Scanning Cloud Radar

1.0 Background

Describe the campaign purpose and scope. Please include the ARM site used for the campaign, the dates or duration of the campaign, the collaborating agencies, principal- and co-investigators as well as additional team members and their affiliations.

Note to Reader: the subsequent description is an updated version of what is stated within the LASIC Science plan

1. Introduction

The southeast Atlantic net cloud radiative forcing attains a global maximum on par with that of the southeast Pacific (*Lin et al., 2010;* Fig. 1). Southerly near-surface winds stream equatorward after their anticyclonic rotation around the south Atlantic sea level pressure high. Lower free-tropospheric winds (~700 hPa), in contrast, are primarily driven by a deeper anticyclone based over southern Africa. These warm winds combine with the cool sea surface temperatures to encourage the formation of a large stratocumulus deck, transitioning to year-round trade-wind shallow cumulus at the location of Ascension Island (14.5^{0}W, 8^{0}S; Fig. 1). This remote but populated volcanic island is the location selected for the ARM Mobile Facility 1 deployment from June 1, 2016-May 31, 2017.

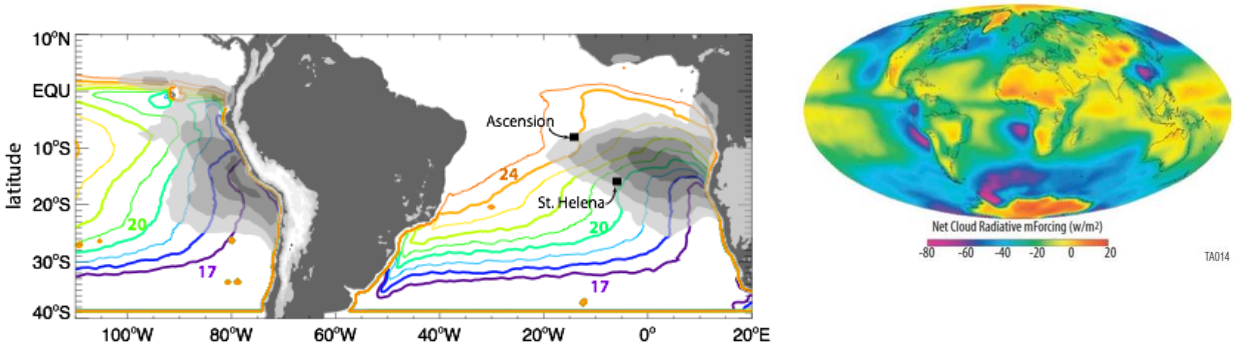

Fig 1: Left-hand panel: The September-mean SST and cloud fraction highlights the large southeast Atlantic stratocumulus region. SST from 1998-2013 Thematic Microwave Imager (labeled colored contour lines in degrees Celsius) and low cloud fraction from 2000-2012 Moderate Resolution Imaging Spectroradiometer (MODIS; grey shading spans 0.6-1). Land topography in 1 km height increments. Right-hand panel: Clouds and Earths' Radiant System (CERES) annual-mean net cloud radiative forcing for March 2000-February 2001, from http://npp.gsfc.nasa.gov.

An unexamined low-cloud regime for DOE/ARM is interactions of shallow clouds with biomass-burning aerosols. Such aerosols absorb as well as scatter shortwave radiation, and shortwave-absorbing aerosols are capable of providing a positive impact on climate (a warming), in contrast to the cooling provided by aerosols, such as sulfate particles, that only scatter shortwave radiation. The separate contribution of biomass burning aerosols to the global climate is highlighted within the Technical Summary of the most recent 2014 IPCC report, where the global radiative forcing is estimated at +0.2-0.5 W m^{-2} (*Boucher et al., 2013*). The contribution to regional climate, particularly over the southeast Atlantic, is much larger.

Global aerosol model estimates of the direct radiative effect of the aerosols alone, even when the aerosol radiative properties are identically prescribed, vary widely, as shown in Fig. 2. The model inter-comparison AeroCom project, an open call to aerosol modeling groups to compare their models

using identical setups, has focused on providing comprehensive assessments of the aerosol life cycle in participating models (*Kinne et al., 2006; Schultz et al., 2006; Textor et al., 2006; Stier et al., 2013; Myrhe et al., 2013*). The AeroCom top-of-atmosphere results demonstrate that, in the mean, the largest positive TOA forcing in the world occurs in the southeast Atlantic, but, that this region also exhibits large differences in magnitude and sign between reputable models. This is also consistent with high variability in the underlying model cloud distributions (*Stier et al., 2013*), and differences in the aerosol vertical distribution (*Koffi et al., 2012*). The AeroCom project is planning a future activity with a focus on biomass burning aerosol effects. *de Graaf (2012)* used high spectral resolution satellite data to show that the instantaneous direct radiative effect of biomass burning (BB) aerosol over clouds in the SE Atlantic region can exceed +130 W m^{-2} instantaneously, and +23 Wm^{-2} in the monthly mean (*de Graaf et al., 2014*). These values are far higher than those diagnosed in climate models, whose monthly-mean regional values reach only +5W m^{-2} (Fig. 2). This suggests a possible universal model underestimate. Underrepresented underlying low cloud albedo provides one plausible explanation.

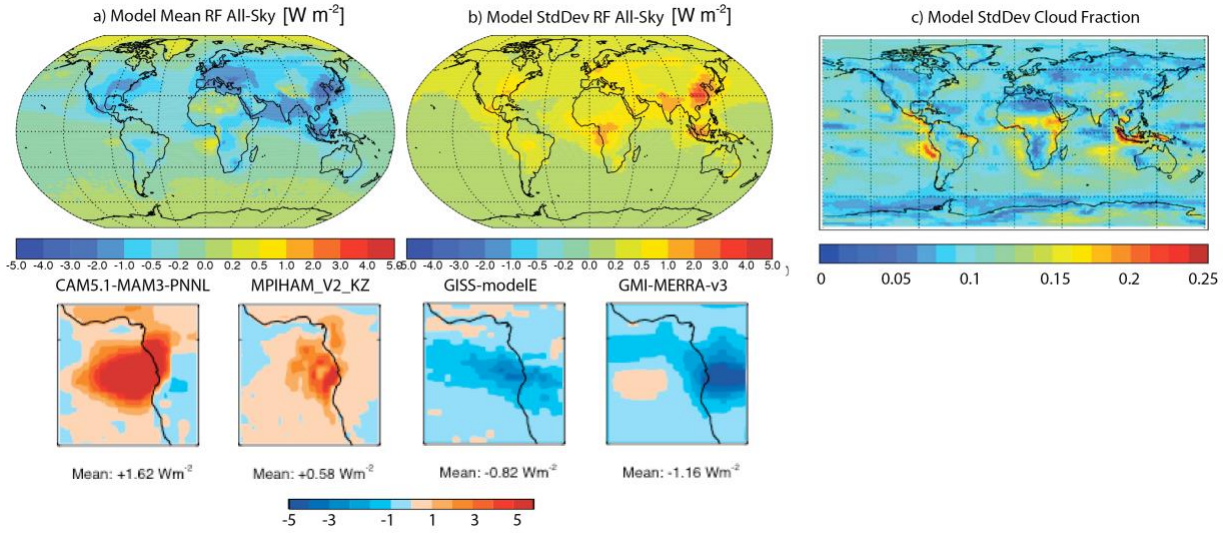

Fig. 2: Estimates of the August-September top-of-atmosphere direct radiative forcing from 12 global aerosol models with prescribed radiative properties (Stier et al., 2013) highlight that a) the largest positive forcing is in the southeast Atlantic, but b) model results vary significantly, c) in part because of differences in cloud fraction.

Ascension island is subject to the free-tropospheric biomass burning (BB) emissions emanating from Africa (Fig. 3). The largest consumption of biomass by fire in the world occurs in Africa (*van der Werf et al., 2006; 2010; Granier et al., 2011*), with the global majority of aerosols overlying clouds occurring in the southeast Atlantic (*Waquet et al., 2013*). The BB aerosol extends well into the trade-wind cumulus region, where the deepening boundary layer and subsiding aerosol layer are more likely to directly interact (Fig. 3, inset). Few observations from the remote southeast Atlantic are available, however, with satellite measurements not yet able to determine the extent to which aerosol is entrained into the boundary layer. Vertical profile data from one UK Met Office research flight to Ascension Island as part of the Southern African Regional science Initiative (SAFARI-UK) in 2000 show enhanced aerosol concentrations within the boundary layer (Fig. 4). Longer-term aerosol statistics, such as will be available from the DOE AMF1 platform, will provide a definitive climatology both at the surface and of the vertical structure, placing such anecdotal evidence on stronger footing.

smoke radiation and composition

At the top of the atmosphere, the direct radiative effect of the biomass burning aerosol is positive (a warming) when the aerosol is located above a bright cloud deck, and negative (a cooling) when above a dark ocean surface (e.g., *Remer, 2009*). For a typical BB aerosol single-scattering albedo (SSA) of 0.9, the cloud fraction above which the aerosol exerts an overall warming has been estimated as approximately 0.4 (*Russell et al., 1997; Abel et al., 2005; Chand et al., 2009; Seidel and Popp, 2012*), based on plane-parallel radiative transfer calculations constrained by satellite data. The cumulus clouds most prevalent at Ascension are not well-modeled radiatively by the plane-parallel assumption, however (e.g., *Zuidema et al., 2008*). It is also worth stressing that small changes in aerosol SSA have a disproportionate impact on the sign of the net top-of-atmosphere radiative forcing (*Haywood and Shine*, *1995*). How the absorbing aerosol ages during transport, thereby affecting the SSA, is not well-known, with current surface-based remote sensing characterization limited to the AERONET site at Ascension Island (*Satheesh et al., 2009*). The comparison of the SSA deduced from the in-situ profile shown in Fig. 4, to those over mainland Africa would estimate that the single-scattering albedo increases from 0.84 over mainland Africa, to 0.91 during the week-long transit to Ascension (*Haywood et al., 2003*).

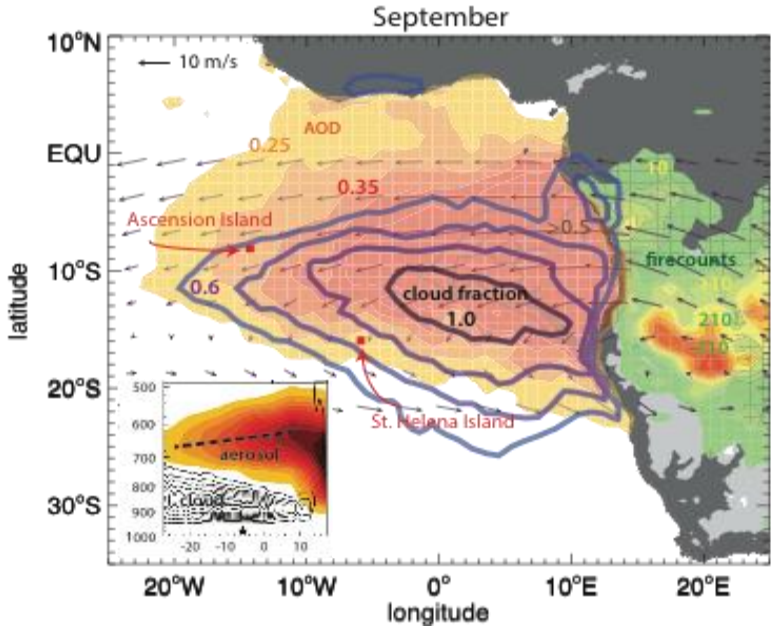

Fig. 3: During September, 600 hPa winds escort the BB aerosol (optical depth in warm colors) from fires in continental Africa (green to red, firecounts) westward over the entire south Atlantic stratocumulus deck (cloud fraction in blue contours). The inset, a 6S-17S longitude slice, highlights the main aerosol outflow occurring at 10S, subsiding to the north where the boundary layer also deepens. Main figure is based on MODIS 2002-2012 data and the ERA-Interim Reanalysis, inset on the space-based Cloud Aerosol Lidar with Orthogonal Polarization (CALIOP) and CloudSat 2006-2010 data. Reproduced from Zuidema et al. 2016.

Most of the black carbon emanating from Africa is released by the open burning of grasslands, with incomplete combustion the norm (*Bond et al., 2013)*. The emissions are thought to be accompanied by large organic aerosol components that also contribute to shortwave and ultra-violet absorption, with the fractional attribution uncertain. The mass absorption cross-section for black carbon can thereby increase by approximately 50% as the black carbon becomes internally mixed with other aerosols. AERONET SSA measurements over land also show a seasonal evolution of SSA from 0.85 to near 0.9 (*Eck et al., 2013*), attributed to changes in fuel types as the biomass burning shifts further to the south. The change of the net radiative properties of the biomass burning aerosol from July to November is therefore also poorly known. The unprecedented sampling throughout the full annual cycle afforded by LASIC will answer the question of whether and how the radiative properties of the smoke evolve offshore as well as over land.

smoke-cloud interactions

As the BB aerosol flows out over the Atlantic ocean, remarkable and poorly-understood interactions with the low clouds occur. These depend crucially on the relative vertical location of the BB aerosol to the cloud deck. When the smoke is situated directly above the cloud field, the stabilization of the atmosphere through warming further supports the cloud field, thickening the cloud and increasing the cloud fraction (*Johnson et al., 2004*). Such a cloud adjustment appears to find observational support in satellite analyses (*Loeb and Schuster, 2008; Wilcox, 2010; 2012; Adebiyi et al., 2014)*. The enhanced cloudiness constitutes a potentially substantial contribution to the net effective radiative forcing that exceeds that from the aerosol alone, capable of increasing the surface cooling from ~0.2K to 2K (*Sakaeda et al., 2011*). An almost-unexplored process issue, however, is the mechanism by which atmospheric warming and aerosol scattering that is maximized at the level of maximum aerosol density at ~650 hPa, is transmitted to the boundary layer cloud residing ~200 hPa below. The impact of shortwave attenuation by aerosol scattering upon the cloudy boundary layer, for example by discouraging decoupling within the boundary layer, as well as the longwave impact of the anomalous moisture present within the aerosol layer (*Adebiyi et al., 2015*), should also be considered.

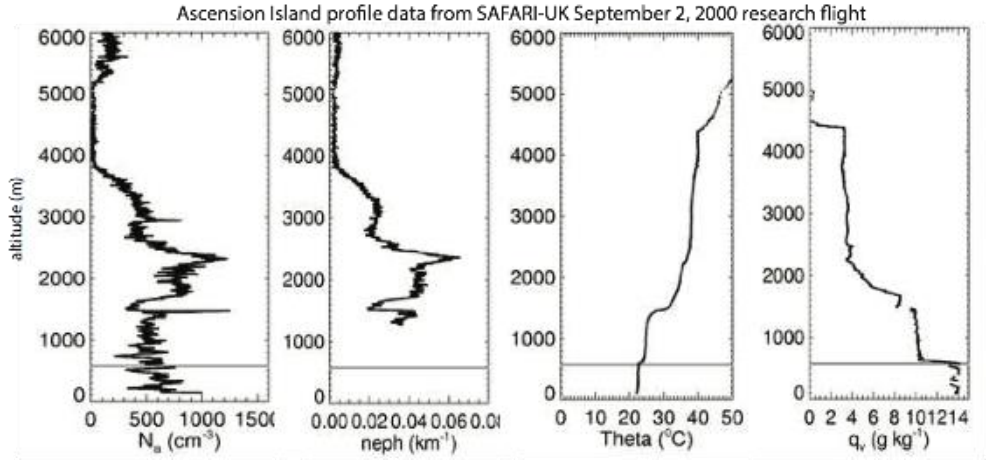

Fig. 4, from left to right: vertical profiles of PCASP accumulation-mode aerosol concentration and the nephelometer scattering coefficient at 0.55 micron indicate aerosol concentrations exceeding 500 cm^{-3} in the boundary layer, with the potential temperature and water vapor mixing ratio profiles indicating two well-mixed layers. The grey line indicates cloud base height. Data sampled while descending near Ascension Island on September 2, 2000, courtesy of Steve Abel, UK Met Office.

If the BB aerosol is located within the cloudy boundary layer, the shortwave absorption warms the cloud and surrounding atmosphere, lowering the relative humidity and thereby the cloudiness (*Ackerman et al., 2000; Johnson et al., 2004; McFarquhar and Wang, 2006; Hill and Dobbie, 2008; Koch and Del Genio, 2010*). BB aerosols can also become entrained into the clouds themselves. While black carbon is hydrophobic, other aerosols, particularly organic aerosols, coalesce with the black carbon during transport and increase its hygroscopicity and thereby effectiveness as a cloud condensation nuclei. Cloud processes such as nucleation and impact scavenging in turn affect the aerosol mass, and feedback further into the ability of the aerosol to act as a cloud condensation nuclei. Results from the SAFARI campaign indeed suggest that CCN increase in aged BB plumes (*Ross et al., 2003*). The activated aerosol can then provide a radiative forcing through their reduction of the mean dropsize, all else held constant (*Twomey, 1977*). There is large-scale evidence of altered microphysics from BB aerosol in the southeast Atlantic from satellite analyses (*Constantino and Breon, 2010; 2013, Painemal et al., 2014*).

The activated aerosol can also affect the likelihood of precipitation (e.g., *Feingold and Seibert, 2009; Wang et al., 2010; Terai et al., 2012*). From DOE measurements collected in the Azores, the rainrate at cloudless R_{cb} is proportional to liquid water path LWP as $LWP^{1.68\pm0.05}$ with an assumed supersaturation of 0.55% (*Mann et al., 2014*). How these exponents change when absorbing smoke particles become the dominant aerosol type, and whether models reproduce these power relationships well are of great interest. Additionally, the precipitation susceptibility to the cloud condensation nuclei number (N_{CCN}) ranges between 0.5 and 0.9 and generally decreases with LWP (as shown in Fig. 5a). Precipitation susceptibility estimates are not yet known reliably for clouds impacted by long-range BB aerosol transport. Measurements from LASIC will provide an excellent opportunity to enhance analysis and intercomparisons of precipitation susceptibility to other aerosol proxies (such as aerosol optical depth, and aerosol index), and to help resolve outstanding discrepancies among various studies.

The susceptibility of precipitation of probability (POP) to N_{CCN} (S_{POP}) also varies between observations from ground-based and aircraft deployments (Fig. 5b) and satellites and simulations (Fig. 5c). S_{POP} from AMF data is higher than that derived from CloudSat, and equivalent with that from aircraft observations (Fig. 5b) and high-resolution simulations (Fig. 5c). This indicates that the high-resolution multi-scale climate model may have already had the ability to represent aerosol-cloud-precipitation interactions properly. More experiments such as intercomparison between high-resolution ground-based measurements and simulations over other sites for a longer time period will provide further valuable confirmation. Ultimately this focus can be used to improve global models; these currently significantly overestimate drizzle frequency, calling into question the fidelity with which the second indirect effect of aerosol is captured.

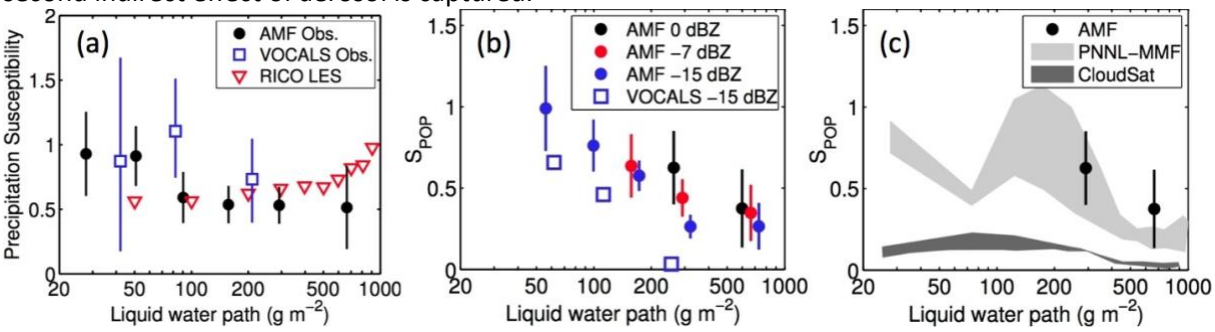

Fig. 5: a) Precipitation susceptibility as a function of LWP in AMF data (with respect to N_{CCN}) and from VOCALS and RICO LES datasets (w.r.t. N_d; Terai et al., 2012; Sorooshian et al., 2009). Susceptibility of POP (S_{POP}) from b) AMF data and VOCALS, and c) CloudSat data and PNNL-MMF outputs at 4-km resolution (Wang et al., 2012).

For BB aerosol, the indirect effects must be compared in relative magnitude against at times opposing semi-direct effects, if, e.g., clouds are brightened as their cloud dropsizes decrease, but overall cloud fractions decrease (e.g., *McFarquhar et al., 2004b; Johnson, 2005*). The recent availability of scanning cloud radars within the DOE mobile deployment pool raises the intriguing possibility that 'cloud burn-off' and changes in microphysics can be simultaneously observed as a function of the boundary layer absorbing aerosol concentration.

2. LASIC Activities, Goals, Hypotheses and Instrument Tables

LASIC (Layered Atlantic Smoke Interactions with Clouds) proposes four activities: 1) to improve current knowledge on the aging during transport of biomass burning aerosol radiative properties as a

function of the seasonal cycle; 2) to establish the aerosol-cloud vertical structure; 3) to improve our understanding of the cloud adjustments to the presence of shortwave-absorbing aerosol within the vertical column, both through aerosol-radiation and aerosol-cloud interactions; 4) to provide observations aiding low cloud parameterization efforts for climate models. Aerosol-free conditions within the measurements of the full annual cycle provide a reference state, and the mean evolution of smoke properties will be evaluated between July to November. The LASIC campaign consists of a deployment of AMF1 instrumentation (the Mobile Aerosol Observing System and ground-based remote sensors) from June 1, 2016 through October 31, 2017 (see Table 1 for a complete list of instrumentation). An **Intensive Observing Period** consisting of 8x/daily radiosondes for two months is designated to coincide with the UK and NASA aircraft deployments (detailed further below) and with the highest aerosol loading, from August 1-September 31, 2016. This characterization of the diurnal cycle of the boundary layer thermodynamic and kinematic vertical structure is unprecedented for the southeast Atlantic. This characterization will be maintained at 4x/daily radiosondes during the rest of the deployment.

LASIC scientific goals are articulated through the following hypotheses:

Hypothesis 1 (H1): The single-scattering albedo of the carbonaceous aerosol overlying Ascension increases during the BB season as has been documented over land.

Hypothesis 2 (H2): Low cloud properties at Ascension vary as a function of the amount, vertical distribution, and optical properties of absorbing aerosol aloft that is distinct from meteorology.

Hypothesis 3 (H3): Carbonaceous aerosol are present within the Ascension Island boundary layer, where they are capable of affecting cloud microphysics, precipitation susceptibility, and the cloud mesoscale organization.

Hypothesis 4 (H4): The evolution of the cloudy boundary layer between St. Helena and Ascension Island varies as a function of the absorbing aerosol loadings aloft as well as large-scale environmental parameters such as sea surface temperature.

LASIC science goals and objectives will be achieved by:

1. Characterizing the microphysical and optical properties of the carbonaceous aerosol at Ascension Island as a function of time.
2. Characterizing the low cloud properties at Ascension Island as a function of the vertical location and optical properties of the absorbing aerosol within the atmospheric column, controlled for thermodynamic state and prior cloud evolution.
3. When carbonaceous aerosol is present within the boundary layer, assessing the aerosol size distribution and hygroscopicity, and relating the aerosol properties to the cloud spatial distribution, its microphysics, precipitation susceptibility, and cloud mesoscale organization.
4. Assessing the evolution of the cloudy boundary layer from St. Helena to Ascension Island under a wide range of atmospheric aerosol conditions as well as large-scale environmental conditions.

Table 1: AMF1 instrumentation	
MAOS baseline instrument	**function**
MAOS-Aerosol (MAOS-A)	
Sonic Detection and Randing (SODAR) System	wind velocity in the lower atmosphere
Ultra-High Sensitivity Aerosol Spectrometer (UHSAS)*	aerosol size and number, 50 nm-1micron
dual-column CCN counter*	# of activated aerosols at 2 supersaturations
single-particle soot photometer (SP2)*	black carbon mass and size
Scanning Mobility Particle Sizer (SMPS)*	aerosol size distribution, 15-450nm
Photo-Accoustic Soot Photometer (PSAP)*	aerosol absorption and scattering coefficient at 3 wavelengths
Humidigraph (scanning RH w/ 3 single-wavelength nephelometers)*	aerosol scattering coefficient as a function of relative humidity
Nephelometer, 3 wavelength*	aerosol scattering coefficient
condensation particle counter (CPC)*	condensation particle concentration, 10nm->3000 nm particle size
condensation particle counter (CPC2)*	condensation particle concentration, 2.5 nm->3000nm particle size
Hygroscopic tandem differential mobility analyzer (HTDMA)*	aerosol growth factor as function of humidity
Particle Soot Absorption Photometer (PSAP)*	aerosol extinction/absorption (black carbon)
7-wavelength aethelometer (AETH)*	aerosol extinction/absorption (black carbon)
weather transmitter (WXT-520)*	T, RH, u, v, rainfall, p
aerosol chemistry speciation monitor (ACSM)*	aerosol mass and composition
radar wind profiler (RWP) (if available)	wind vertical structure
MAOS-Chemistry (MAOS-C)	
trace gas instrument system*	CO, SO2, NO/NO2/NOy, O3
proton transfer mass spectrometer (PTRMS)*	volatile organic compounds

AMF1	
3-channel microwave radiometer (MWR3C)*	integrated liquid water and water vapor
balloon-borne sounding system (SONDE)* 4x/daily increasing to 8x/daily for 2 months	temperature, humidity and wind vertical structure
ceilometer (VCEIL)*	cloud base
radar wind profiler (RWP)*	wind vertical structure
W-band scanning cloud radar (WSACR)*	cloud and precipitation spatial structure
W-band zenith cloud radar (WACR)*	cloud and precipitation vertical structure
K-band scanning cloud radar (KASACR)*	cloud and precipitation spatial structure
micropulse lidar (MPL)*	aerosol vertical structure
atmospheric emitted radiance interferometer (AERI)*	cloud liquid water path and effective radii
multifilter rotating shadowband radiometer (MFRSR)*	aerosol optical depth
Narrow Field of View (NFOV)*	cloud optical depth and effective radius
solar array spectrometer (SASHE & SASZE)*	radiative closure
surface energy balance system (SEBS)*	surface energy balance. soil moisture and flux measurements are not needed.
surface radiation measurements (SKYRAD, MFR, GNDRAD)*	surface radiation balance (overlap with SEBS?)
meteorological instrumentation (MET)*	surface air layer properties
optical rain gauge (ORG)*	surface rain
tower camera (TWRCAM)*	photo imagery
total-sky camera (TSI)*	cloud fraction

Table 1 lists the specific AMF1 instrumentation requests for Ascension. These include the MAOS-Aerosol and MAOS-Chemistry (MAOS-A and MAOS-C) packages, which we anticipate will be relocated directly from the GoAmazon deployment in Brazil to Ascension Island. Priority instruments are identified through an asterisk. Further planning details, including additional anticipated and desired instrumentation, and campaign-specific priorities including Value-Added Products (VAPs) are contained in Section 4.

3. Specific Objectives

3.1: Characterizing aged carbonaceous aerosol (H1)

Most biomass burning aerosol measurements are taken close to their source. Yet, the carbonaceous aerosol that alter the radiative fluxes and heating rates over the Atlantic ocean are already aged by at least a day, with the transport time to Ascension taking 5-6 day (*Adebiyi and Zuidema, 2016*). In-situ characterization during SAFARI-2000 concluded that most of the aerosol aging occurs within the first few hours after leaving the source region (*Abel et al., 2003*), with the SSA rising by 5% over that time. *Vakkari et al. (2014)* similarly find that atmospheric oxidation and subsequent secondary aerosol formation drive large changes in BBA properties in the first 2-4 hours of transport. However, a satellite-based study suggests BB aerosol sizes and thereby the SSA continue to evolve during aerosol transport over the Atlantic (*Waquet et al., 2013*). Ascension is 3000 km away from the African coast, and as such the comprehensive surface-based aerosol measurements possible with the Mobile Aerosol Observing system will assess the properties of the truly aged aerosol. Because the characterization is occurring so far from the biomass burning source, these surface-based aerosol characterizations can be considered representative of the carbonaceous aerosol properties throughout the vertical column. These surface-based measurements will characterize those properties of BB aerosols most needed to model the direct radiative forcing: the mass absorption and scattering cross-sections and mass concentrations. Measurements specifically aimed at characterizing the aerosol SSA include the photo-acoustic soot spectrometer (PASS), the Particle Soot Absorption Photometer (PSAP), the seven-wavelength aethelometer, and the humidigraph. The latter is able to assess the aerosol scattering coefficient using three different wavelength nephelometers as a function of relative humidity.

Closure studies will link absorption to measurements of BC mass and mixing state, such as from the single-particle soot photometer (SP2) and aerosol chemistry speciation monitor (ACSM). Column radiative closure studies with the MFRSR and SAS-Ze on cloud-free days, alone or in combination with aerosol vertical profile information from the MPL (see Section 3.3), will characterize the column-average aerosol properties needed to match the observed surface radiance and thus provide information on the aerosol aloft. This work goes hand-in-hand with developing retrievals for the SAS-Ze and SAS-He spectral radiometers. The LASIC observations will provide an independent opportunity to evaluate the ARM 3-wavelength Aerosol Best Estimate (ABE). This will be done by comparing calculations from the LBLRTM/CHARTS radiative transfer model (*Mlawer et al., 2000)* using the ABE profiles as inputs, to the observations of the SAS-Ze and SAS-He spectral radiometers near the ABE reference wavelengths. The SAS-Ze and SAS-He measurements will also lend themselves to better estimates of AOD, SSA, and g. Since these properties are largely determined by the aerosol composition and size distribution, the strategy is to determine the column-integrated aerosol size distribution and complex index of refraction (which is a function of aerosol composition) that is most consistent with the available SAS-Ze and SAS-He data, similar to the method of *Kassianov et al. (2007)* for the ARM MFRSR. Further co-located measurements of aerosol chemical composition, size distribution, and optical properties, along with knowledge of sources and air transport, will be evaluated in relation to column and profile properties from ground-based passive and active remote sensors, providing a fuller and more accurate characterization of the aerosol throughout the column.

Further measurements will assess the ability of the aerosol to act as a cloud condensation nuclei, with an ultra high sensitivity aerosol spectrometer (UHSAS) as well as a Scanning Mobility Particle Sizer (SMPS) providing the sizing over the dominant CN size ranges (50-1000 nm and 15 nm-450 nm, respectively). Such datasets will be combined with a dual-column cloud condensation nuclei counter capable of counting the number of aerosols activated into CCN at two representative and independently-selected supersaturations. Such measurements are integral to providing constraints for aerosol-cloud modeling, including for the Aerocom project. In addition, efforts will be made to analyze the chemistry of the carbonaneous aerosol. This will be done using the updated Aerosol Simulation Program (ASP), with updated gas-phase chemistry and the Volatility Basis Set (VBS) scheme for SOA

Fig. 6: CALIOP snapshots of 532 micron backscattered intensity near Ascension Island suggests a range of cloud-aerosol interactions. Ascension's latitudinal location is indicated as a red box on x-axis.

formation (*Alvarado and Prinn, 2009; Alvarado et al., 2014*). This improved ASP version has been used to analyze the chemistry of a South Africa savannah fire smoke plume (*Hobbs et al., 2003*) and the Williams fire smoke plume sampled by *Akagi et al. (2012)*.

3.2: Accurate identification of aerosol-cloud vertical structure (supports H2, H3 and H4)

To first-order, the vertical distribution of the absorbing aerosol and low cloud and their spatial and temporal variability must be known before the radiative forcings and cloud adjustments can be adequately characterized. The importance of an accurate characterization, and our current lack of one, is worth emphasizing. Space-based lidar is currently our best source of information (e.g., Fig. 6). From space, the optically-thin aerosol layer base must be detected after the lidar signal is attenuated by the intervening aerosol. During the day, the vertical sampling is hampered by solar interference, so that retrieved daytime smoke base altitudes are placed 500 m higher in the mean compared to nighttime altitudes (*Meyer et al., 2013*). Thus, CALIOP cloud-aerosol separation statistics tend to suggest little cloud-aerosol overlap and therefore little aerosol entrainment into the cloudy boundary layer (*Meyer et al., 2013*), but, this is contradicted by satellite studies of the clouds themselves (e.g., *Constantino and Breon, 2013; Painemal et al., 2014*), and anecdotally by the available in-situ data such as shown in Fig. 4.

A definitive climatology of how often free-tropospheric aerosol interact with clouds rooted within the boundary layer requires long-term, high-time-resolution surface-based lidars and radars. These provide much more detailed and vertically-resolved profiles of aerosol and clouds than is possible from space. The aerosol vertical structure statistics also further our understanding of the transport and eventual deposition patterns of BB aerosol. The AMF1 micropulse cloud lidar (MPL) will be able to resolve the vertical structure to 30 m. Ascension Island is already an AERONET site, and the DOE MPL dataset can potentially contribute constructively to a merged dataset with the AERONET data. This will require coordination with MPLNET protocols (*Welton et al., 2001*). The surface-based W-band zenith radar (WACR) primarily, and the scanning Ka-band and W-band cloud radars (KASACR and WSACR) provide an accurate view of the cloud and precipitation vertical structure, resolved to 50 m, that will then be integrated with the lidar-derived aerosol statistics.

3.3: Cloud adjustments to aerosol-radiation and aerosol-cloud interactions (H2,H3)

If the surface-based aerosol measurements and vertically-profiling lidar indicate that BB aerosol is present within the cloudy boundary layer, the DOE measurements will support scientific inquiry into the resulting cloud adjustments. These include what has colloquially been referred to as the "cloud burn-off" effect, whereby shortwave absorption by the aerosol raises the local temperature, reducing

the relative humidity, and discouraging cloud growth. If this effect is also induced by BB aerosols entrained into boundary layer cloud drops, a reduction in the mean drop size can occur for the same liquid water content, potentially reducing precipitation or enhancing evaporation even further. To date, the impact of entrained BB aerosol in the boundary layer has been examined for INDOEX data (*Ackerman et al., 2000*) and the Amazon (e.g., *Feingold et al., 2005*). In both field experiments, the smoke was already present within the boundary layer.

The hyper spectral irradiance and radiance measurements from the scanning spectral Solar Array Spectrometer-Hemispheric and -Zenith (SASHE and SASZE) radiometers in the visible and near-infrared (NIR) regions will be applied to help separate the respective aerosol-cloud signatures. The NIR wavelengths are able to reveal much more cloud fine structure than the visible wavelengths, mainly because the higher NIR-absorption by liquid water reduces the radiative smoothing effect of cloud multiple scattering. The better knowledge of cloud properties from the NIR wavelengths can then improve the characterization of aerosol optical properties towards achieving radiation closure.

Such measurements, when combined with the dual-wavelength scanning Ka-band and W-band cloud radars (KASACR and WSACR) and with longer-term instruments possessing well-characterized retrieval algorithms, such as the Multifilter Rotating Shadowband Radiometer (MFRSR), Microwave Radiometer Profiler (MWRP), and a 3-channel and high-frequency Microwave Radiometer (MWR3C and MWRHF), are well-poised to provide insight into the relative magnitude of competing radiative effects from aerosols and clouds. The net radiative impact will be succinctly summarized by the Downwelling Radiation (SKYRAD) and Surface Energy Balance System (SEBS) measurements, and surface-based rain gauges will assess how much precipitation reaches the surface and leaves the atmosphere. Precipitation susceptibility estimates can then be generated using the WACR-derived precipitation estimates, microwave-derived liquid water path, and the CCN-counter concentration values and other aerosol proxies.

As noted previously, such susceptibility metrics have been found to systematically differ from those derived using space-based remote sensing at larger scales (Fig. 5), with implication for how these metrics are used to parameterize climate models. The long-term statistics from Ascension Island, occurring within a different aerosol-cloud regime, will provide an opportunity to test the universality of these results. These observational efforts will be coordinated with high-resolution modeling of aerosol-cloud processes.

The precipitation particle size distributions from the Joss-Waldvogel disdrometer and the optical rain gauge rainfall rate measurements will furthermore be used to adjust (calibrate) the radar wind profiler (RWP) power measurements using the techniques developed by *Tridon et al., 2013*. Using the newly proposed RWP operational modes we will have cloud and precipitation observations from the surface throughout the full depth of the atmosphere with no attenuation. Combining the RWP with the WACR observations will provide a dual-wavelength view of clouds and precipitation. The RWP will also contiguously map the inversion height (compared to the 4-8 daily measurements from the soundings) and help identify the entrainment episodes of free tropospheric air that are so critical for bringing in smoky free-tropospheric air into the boundary layer.

The Ka/W- scanning ARM cloud radars (*Kollias et al., 2014a*) will provide information on the mesoscale structure and organization of the cloud fields (*Kollias et al., 2014b*), including on the horizontal wind fields in the cloud layer. The Ka/W-SACR will be used to track cloud structures and study the lifetime of isolated cumuli clouds (*Borque et al., 2014*). The recorded radar Doppler spectra can be used to assess the early drizzle growth (*Kollias et al., 2011a; 2011b*) as a function of variable aerosol conditions. From the constructed 3D cloud structure (*Lamer et al., 2013*), the 3D vertical velocity field can be retrieved and applied to entrainment studies using the profiling and scanning cloud radar observations.

When the absorbing aerosol layer is entirely located above the cloud, the stabilization of the atmosphere at that level may encourage cloudiness by discouraging the entrainment of warmer, drier air into the boundary layer. The absorbing aerosol layer aloft is typically associated with anomalous moisture (*Adebiyi et al., 2015*), aiding hygroscopic growth of the aerosol that further increases its ability to scatter shortwave radiation. The moisture-swelled aerosol attenuates the shortwave radiation reaching the cloud, while the longwave opacity of the moisture will diminish the cloud-top longwave cooling. All else equal, solar-induced decoupling should be reduced within the boundary layer when absorbing aerosol is present overhead, fostering a more well-mixed boundary layer. On the other hand, the reduced cloudtop long-wave cooling will drive less turbulence within the boundary layer, providing the opposite feedback. Thus, the inference of the cloudy boundary layer adjustments to free-tropospheric aerosol loadings will require knowledge of the boundary layer decoupling. The Balloon-borne Sounding System (SONDE) datasets will be applied to assess boundary layer decoupling throughout the annual cycle. WACR radar data will help distinguish the impact of turbulent mixing from microphysics upon the spectrum width (e.g., *Fang et al., 2012*). The evolution of the boundary layer will also be characterized using a new AERI-based retrieval that is able to infer temperature and humidity profiles at high time resolution from both clear and cloudy-sky scences (*Turner et al., 2014*).

A vertical profile of aerosol extinction can be inferred from the lidar backscattered intensity using AERONET or other aerosol optical depths as a constraint. The SSA will be determined from the surface aerosol measurements and assumed to represent the entire column. The cloud optical depth can be inferred from NFOV or sun photometer zenith radiance measurements (*Chiu et al., 2012*). From these inputs, estimates of the aerosol heating rates can then be calculated. When clouds are inhomogeneous, radiative transfer results can be filtered for spectrally-consistent data that can be compared to SASZE and SASHE measurements, similar to what has been done with aircraft-based Solar Spectral Flux Radiometer (*Kindel et al., 2011*). When the aerosols are embedded within the cloud layer, a similar statistical combination of modeling and measurements can quantify the heating rates (*Schmidt et al., 2009*). Competing radiative impacts from changes in microphysics and cloud spatial organization can be discriminated using three-dimensional radiative transfer modeling of large-eddy simulations initialized by the observations and compared to measured irradiances (*Zuidema et al., 2008; Schmidt et al., 2009*). Such radiative closure provides a means of not only assessing retrieval accuracy, but also for extrapolating local observations with confidence to larger scales. This represents a significant opportunity for satellite retrieval development and assessment within a difficulty space-based remote sensing regime.

3.4: Distinguishing aerosol from meteorological effects (H2, H4)

A first-order activity is to understand the depth and complexity of the well-coupled aerosol-meteorological state. It is imperative that the meteorology be well-characterized, towards constraining modeling simulations and confidently distinguishing aerosol effects. As much will be done prior to the campaign as possible. Burning over continental Africa occurs throughout the full year, but the circulation pattern that favors the westward advection of the aerosol occurs primarily between July to November, and is most pronounced in September-October. At this time the aerosol-bearing southerly African easterly jet (*Jackson et al., 2009*), centered at approximately 10^0 S, or near the latitude of Ascension Island, is most pronounced (*Adebiyi and Zuidema, 2016*). This outflow is accompanied by moisture that also influences the cloudy boundary layer. Boundary layer clouds are known to be highly influenced by boundary-layer conditions prevailing 24-36 hours upstream (e.g., *Klein et al., 1997; Mauger and Norris, 2007*), which for Ascension Island occurs southeast of the island. Thus, unlike the

southeastern Pacific, a strong wind shear exists between the free-tropospheric and boundary layer winds (compare, e.g., Fig. 1 with Fig. 3).

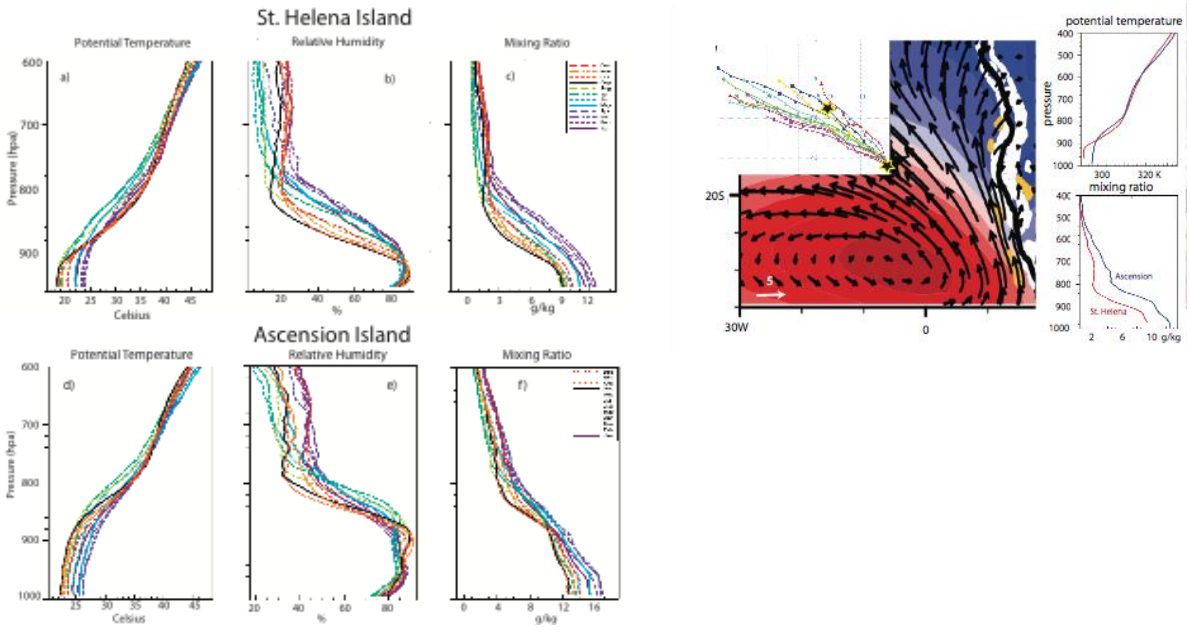

Fig. 7: a)-g) Monthly-mean profiles of atmospheric potential temperature, relative humidity and mixing ratio clearly highlight the warmer, deeper and moister boundary layer at Ascension Island (bottom row) compared to St. Helena (top row), and the distinct seasonal cycle at each location. from 2000-2012 IGRA soundings (radiosondes were discontinued at Ascension Island after 2012). Right panel: Sept-Oct ERA-Interim 1000 hPa climatological winds and sea level pressure with an ensemble of Sept. 2013 HYSPLIT forward trajectories from St. Helena Island (superimposed) passing near Ascension Island, and September-mean thermodynamic profiles from both islands.

The meteorological conditions encouraging aerosol outflow and their dynamical impact on the low cloud fields will be characterized using daily ERA-Interim reanalyses (e.g., *Adebiyi et al., 2015*), with the goal of defining an easy-to-apply meteorological metric associated with the aerosol outflow (e.g., the strength of the southerly African Easterly Jet; *Adebiyi and Zuidema, 2016*). Thermodynamic observations of the entire annual cycle (Fig. 7) confirm that large-scale conditions at Ascension Island are consistently representative of the trade-wind conditions, easing the ability to identify smoky and pristine large-scale conditions with similar thermodynamic context at Ascension. The natural variability of the low cloud fields at Ascension will be examined using satellite data as a function of both the aerosol-associated meteorological metric and the cloud upwind conditions as defined by Reanalysis datasets prior to the campaign. The four-times daily soundings, increasing to eight-times daily during the August-September IOP, combined with a Radar Wind Profiler (RWP) will characterize Ascensions island's wind vertical profile and can help finetune the analysis begun with ERA-Interim datasets. UK Met Office measurements at St. Helena Island, which is upstream of Ascension if considering the boundary-layer winds, but downstream if considering the free-tropospheric winds driving the aerosol outflow, will be related to the DOE measurements at Ascension island.

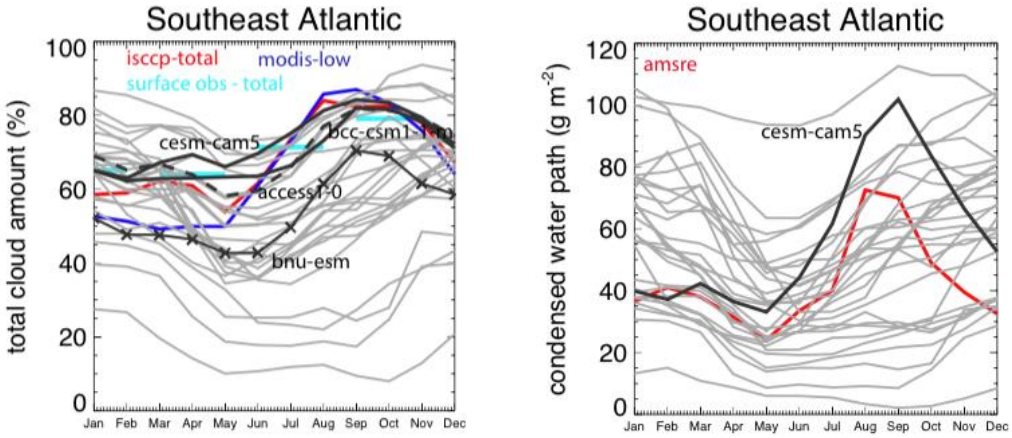

Fig. 8: The annual cycle in left) cloud amount and right) liquid water path over the 10^0-20^0S, 0-10^0E region (Klein and Hartmann, 1993) in CMIP5 models and observations. These include ISCCP, EECRA, and MODIS and AMSR-E (2002-2012). The black lines indicate CMIP5 models with the highest correlations to the observed values. The DOE-supported CESM-CAM5 model depicts the most realistic annual cycle of the models shown, supporting further cloud parameterization activities.

3.5: Measurements that span the full annual cycle and low-cloud model parameterization development support (H2, H4)

The BB aerosol radiative properties will be evaluated at Ascension as a function of time during the July-November BB-burning season. Should the smoke single-scattering albedo be determined to trend systematically at the remote Ascension Island, this will also impact the radiative heating profile. The impact (and frequency) of BB aerosol entrained into the boundary layer may in turn also evolve with time, and will be evaluated. AERONET measurements from the continent and at St. Helena will help determine if and how similar systematic trends typify all of the locations.

The seasonal cycle is also an important metric with which to assess the behavior of low clouds within climate models. Many CMIP5 models exhibit a seasonal cycle in liquid water path that is out-of-phase with the observed seasonal cycle over the main stratocumulus deck (Fig. 8) as defined within Klein and Hartmann (*1993*; 10^0-20^0 S, 0-10^0E). Modeled skill at capturing the annual variation in low cloud fraction has been shown to increase for models with more realistic annual cycles in the lower tropospheric stability (*Noda and Satoh, 2014*), suggesting the problem lies more with the internal cloud parameterizations, than with the climate model depictions of the large-scale state. Ascension and St. Helena Island can serve as foci for more detailed output of the next-generation CMIP6 models, to further diagnose model behavior. A correct seasonal cycle in cloud fraction and cloud properties in both global aerosol models and climate models lacking aerosol representation, is a prerequisite for models seeking to further improve the internal cloud model representation. The concurrent radiosonde thermodynamic profiles combined with cloud property measurements will allow for a sensitive interrogation using a range of models, from process-level large-eddy simulations, to climate models, to further parameterization efforts for low clouds. Efforts will be made to advance modeling foci on low clouds through ensuring and developing the Value-Added Products most useful for Climate Process Teams, the DOE Cloud-Associated Parameterizations Testbed (CAPT), and the DOE Aerosol Modeling Testbed and Large-Eddy Simulation Testbeds. The radiosondes, most particularly during the Intensive Observing Period when radiosondes are launched 8x/day on Ascension, along with more radiosondes launched on St. Helena by the UK Met Office, will provide crucial initialization and evaluation products.

4. Site Description, Planning, Value-Added Products and Collaborations

4.1 Site Description

Ascension Island is governed as part of a larger British Overseas Territory that includes St. Helena and Tristan da Cunha. The island does not maintain a permanent population and a contract of employment is required for residence upon the island, although opportunities for tourism are becoming more available. The UK Royal Air Force and US Air Force both maintain a presence, centered around WideAwake Airfield. The US Air Force presence (~20 personnel) is an auxiliary base of Patrick AFB in Florida, and the island is serviced regularly every 60 days by a US cargo ship, the MV Ascension, making round trips to and from Cape Canaveral, Florida. The island has a history of scientific endeavors because of its unique location. It is used as a rocket tracking station, Anglo-American signals intelligence facility, BBC World Service relay station, and hosts ground antenna that assist in the operation of the Global Positioning System. Radiosondes were launched from Ascension Island with US Government funding until 2012, but no radiosonde launchings have occurred since then. Ascension Island is still an AERONET site. The UK Met Office has used Ascension island as a stop on its ferry flights to and from Africa (e.g., SAFARI), and some limited in-situ data are available from those flights (Fig. 4). On St. Helena, the UK Met Office has been launching almost-daily radiosondes for many decades, archived by them at higher vertical resolution since 2000. The higher vertical resolution is a necessary condition for supporting research into aerosol-cloud-meteorological characterization at St. Helena (*Adebiyi et al., 2015*). Lower-resolution radiosonde data are available for both sites through the IGRA database (Fig. 7).

Ascension is a volcanic remnants with a maximum altitudes of 818 meters. Ascension does not intrude above the cloud-topped boundary layer (Fig. 9), but the island is nevertheless capable of modifying the flow, primarily visible through a wake effect seen in satellite imagery (Fig. 9). This should not affect the surface-based aerosol measurements of mass, composition, and absorption, but the boundary layer flow modification could affect, e.g., the mean cloud fraction and cloud diurnal cycle. The island effects will affect site location choice, and the island impact on cloudiness will need to be assessed. The TSI camera will assess local gradients in the cloud cover. A larger-range option for assessing island effects could be through Unmanned Aerial Vehicles (perhaps through DOE's guest instrumentation program), and to compare aircraft launches and departures to the radiosondes. A satellite approach would be to assess cloud retrievals from the Visible Infrared Imaging Radiometer Suite (VIIRS), available at 750 m resolution but only at regular times, combined with cloud retrievals from the diurnally-resolving geostationary SEVIRI instrument. Such analysis is anticipated as part of the effort to distinguish meteorological effects already (see Section 3.4). A topographic map indicating developed roads and sites is included in Appendix A, with the digital image available at http://www.rsmas.miami.edu/users/pzuidema/Ascension_map.pdf.

The anticipated distribution of instrumentation is indicated in Fig. 10. The AMF1/MAOS will be located at 365 m on the windward side. Its distance from the airport and from other habitation is intended to secure aerosol measurements typical of off-shore. The necessary power generator will be located as far away, upwind, from the instruments as possible. The radiosondes will be launched from the airport, adding to a previous long time series. A microwave radiometer will also be placed there, augmenting a ceilometer and an AERONET site that are already placed there.

4.2 Related Campaigns

Complementary activities were conducted by the UK Met Office and NASA. The UK Met Office Cloud-Aerosol-Radiation Interactions and Forcing: Year 2017 (CLARIFY; PI: Jim Haywood) deployment of its FAAM BAe-146 plane from Ascension spans mid-August to mid-September of 2017. The NASA

ORACLES (Observations of Aerosols above Clouds and their Interactions, PI: Jens Redemann, NASA AMES; Deputy PI: Rob Wood) is a multi-year multi-aircraft deployment. It was based out of Walvis Bay, Namibia in September, 2016, and Sao Tome in August 2017 (and will be late September through late October, 2018). ORACLES deployed the P-3 and ER-2 planes in 2016, and the P-3 alone in 2017 and 2018. NASA also established a new AERONET site upon St. Helena in 2016. The French AEROCLO-Sa campaign, PI: Paola Formenti) deployed a Falcon plane out of Walvis Bay in August, 2017 and augmented its surface measurements in Henties Bay, Namibia.

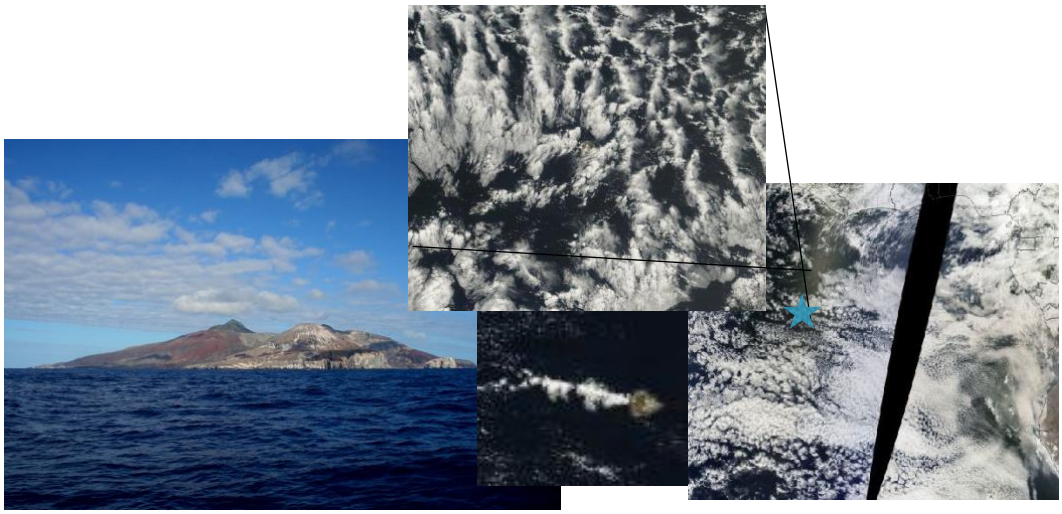

Fig. 9, leftmost panel: Ascension Island seen in profile. The rightmost panel indicates the location of Ascension within the southeast Atlantic using MODIS satellite imagery from September 4, 2013, with an expanded view centered upon Ascension (blue star) in the top middle panel. CALIOP imagery from the next day (Fig. 5) indicates the presence of smoke. The bottom middle panel shows an example of the island wake effect, from Sept. 30, 2013.

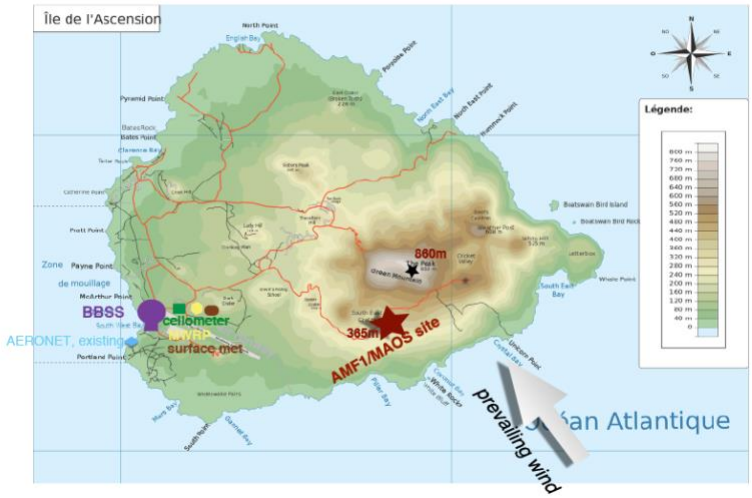

Fig. 10: Ascension Island layout of instrumentation.

The UK CLARIFY similarly

investigated the direct, semi-direct and indirect effects of biomass burning aerosols over the SE Atlantic. CLARIFY will focus on using its measurements to immediately improve the UK Met Office model, which has incorporated the GLOMAP-mode state-of-the-science aerosol model (*Mann et al., 2010; Bellouin et al., 2013*). The UK suite of remote sensors will provide the upwind (boundary layer) and downwind (free-tropospheric) information on the evolution of cloud and aerosol properties that are also being sampled at Ascension. The lead investigator Dr. Jim Haywood, a co-investigator on LASIC, will facilitate coordination and data-sharing between the projects. The unified UK Met Office operational forecast model will be applied at 4km resolution for the campaign, with the forecasts shared between all campaigns. Post-campaign modeling exercises are anticipated to incorporate the datasets from all campaigns. Meteorological forecasts done in the context of CLARIFY will be tested with LASIC datasets.

The NASA ORACLES (Observations of Aerosols above Clouds and their Interactions, http://espo.nasa.gov/oracles; PI: Jens Redemann, NASA AMES; Deputy PI: Rob Wood) project will overlap with the CLARIFY campaign in 2016, during which time the NASA P-3 plane will also be based out of Walvis Bay, Namibia. ORACLES focuses on using airborne remote sensing tools that are important to future NASA satellite missions. The NASA P-3 plane will host aerosol and cloud in-situ instrumentation, including a high-spectral resolution lidar (HSRL-2), cloud radars, and solar spectral flux radiometers (SSFR and 4STAR). Most of the CLARIFY and ORACLES research flights will take place closer to the Namibian coast, both upstream (boundary layer) and downstream (free-troposphere) of the airflow encountering Ascension. ORACLES will study intraseasonal variations (August to October) in aerosol and cloud properties and their interaction, in three campaigns between 2016 and 2018. The NASA P-3 plane was supplemented by the ER-2 plane in 2016, which will include remote sensing (HSRL-2, enhanced MODIS Airborne Simulator (eMAS), Airborne Multiangle SpectroPolarimeter Imager (AirMSPI), and an SSFR).

The NASA ORACLES deployed its P-3 plane to equatorial Sao Tome Island (6.5^0E), in the Gulf of Guinea, in August of 2017. This situated the plane near the aerosol exiting continental Africa, and over warmer waters encouraging deeper boundary layers, enhancing the sampling for smoke-cloud microphysical interactions. Half of the flights were devoted to survey flights along 5^0 E between the equator and 15^o S. A "suitcase" brought the C-130 to Ascension Island and also allowed the plane to do some sampling of the offshore boundary layer unobstructed by the island.

A larger Scientific Coordination Group, composed of the principal investigators and other major personnel, optimized the coordination between the different campaigns. Another possibly complementary science project is the NASA Atmospheric Tomography Mission (PI: Steve Wofsy, Harvard), which undertook/is undertaking four around-the-world research flights in five years with stops in Ascension to understand the chemical processes controlling methane and ozone. A ground station of the Total Carbon Column Observing Network measures all the major greenhouse gases, described at https://tccon-wiki-caltech.edu/Sites/Ascension_Island (PI: Dietrich Feist, MPI-Biogeochemistry).

The LASIC-SSA Constraint Study

The intrinsic radiative property of smoke supporting the absorption, or the single-scattering-albedo (SSA), varies with composition, aging, and hygroscopicity. The SSA is still poorly constrained for smoke emanating from African continental fires after long-range transport. Filter-based techniques such as the Particle Soot Absorption Photometer (PSAP), nephelometers and aethalometers estimate extinction from the change in light transmission through particle-imbibed filters. The Cavity Attenuated Phase Shift (CAPS)-SSA uses entirely different approach. It utilizes a unique optical design to simultaneously measure aerosol light extinction and scattering in the same sample volume. These can then be used to

derive the SSA and aerosol absorption (Onasch et al., 15). The CAPS-SSA absorption estimate will serve as a reference and anchor for the longer-term filter-based measurements, helping to fulfill an important goal of the LASIC campaign and of the ASR Aerosol Working Group. This endeavor is a joint effort between Aerodyne and DOE ARM, and brought the CAPS-SSA monitor out to Ascension from August through September in 2017.

Supplemental Measures for the LASIC Campaign

Supplementary measurements were desired for the LASIC campaign to properly characterize the representativeness of the chosen AMF1/MAOS site, to address the island effect, and to colocate a microwave radiometer at the radiosonde launch site, towards properly constraining the radiosonde humidity profiles.

2.0 Notable Events or Highlights

Include details of unusual or interesting observations, unique meteorological episodes, instrument issues, and/or any other significant events.

The smokiest day of the 17-month-long campaign, recorded at the surface by the single particle soot photometer, occurred on August 13, when the daily-mean black carbon mass concentration almost reached 1700 ng m^{-3}. As described in Zuidema et al., (2018), on 13 August, 2016, closed-cell cumulus clusters with cores reaching 2 km generated upper-level stratiform cloud, with lower local orographically-lifted cloud at the AMF1 site fully attenuating the lidar signal. The following day was characterized by more suppressed wind-aligned shallow cumuli that allowed the micropulse lidar to more fully probe the atmosphere. Smoke was present to above 3 km (Fig. 11a, encompassing 14 August 12 UTC to 16 August 00 UTC). At times, the smoke within the boundary layer almost fully extinguishes the lidar signal (e.g., 14 August 15 UCT), and the ceilometer-derived cloud base heights are included to distinguish aerosol from cloud. The pronounced extinctions coincide with relative humidity maxima, one at approximately 800 m, corresponding to the lifting condensation level, and 1.5 km just below the trade-wind inversion (Fig.11c). These relative humidity profiles indicate a decoupled boundary layer, often observed at Ascension. Both cloud-containing layers are individually well-mixed in moisture (not shown, but consistent with the linear increase in the relative humidity with altitude). The deliquescence of the smoke particles is confirmed by the lower lidar volume depolarization ratios within the boundary layer (Fig.11b) indicative of more spherical particles.

The near-surface water vapor mixing ratio of 12-14 g kg-1 decreases to ~ 3 g kg-1 above the trade-wind inversion (not shown) for a relative humidity of 20-30%. The specific humidity of the upper aerosol layer indicates air that was last saturated at an altitude of approximately 5 km, consistent with the residual of a deep continental boundary layer. The lidar volume depolarization ratio increases, consistent with more desiccated, aspherical aerosol. The higher aerosol layer is resting directly upon the trade-wind inversion, most obvious in Fig.11c; this feature was common to almost all the days with an upper-level smoke layer (visually determined from daily lidar imagery). The lidar extinction values above the cloud layer are considered biased low by a factor of 0.35 and the vertical gradient in extinction reflects attenuation of the lidar signal, as the moisture layer is well-mixed. Either by assuming the extinction just above the cloud layer of 0.1 km-1 is a constant through the aerosol layer, or by correcting by a factor of

2.8 supports an estimate for the above-cloud aerosol optical depth of approximately 0.2 until mid-day 15 August, or almost one-half of the column sun-photometer-derived aerosol optical depth of 0.48 between 15-18 UTC on 14 August.

Radiosonde-derived wind profiles indicate westward winds throughout the entire 0-4 km column during 13-16 August, 2016 (not shown). The 7-day HYSPLIT backtrajectories at 500, 1000 and 2000 m indicate a direct northwestward transport from continental African fire source regions, with the week-long meteorology integrating to bring continental smoke to Ascension Island (Fig.12). This atmospheric boundary layer flow contrasts with the climatological wind pattern of southeasterlies advecting clean southern hemisphere air around the southern Atlantic subtropical anticyclone, apparent on backtrajectories for most other August days (Fig. 12e). 31 August is another day with both high near-surface rBC values and a 500 m backtrajectory tracing back to continental Africa. This flow pattern, previously noted in Swap et al. (1996), is important for explaining high near-surface aerosol loadings, and can also include aerosol transported at a slightly higher altitude (~ 1 km) that becomes entrained into the boundary layer further offshore.

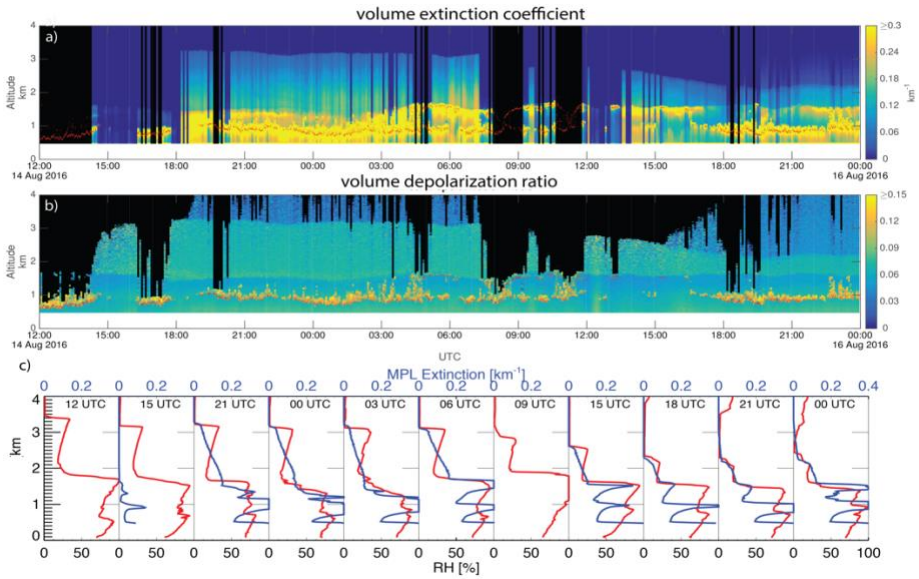

Fig. 11: 14 August 1200 UTC - 16 August 00 UTC time series of the micropulse-lidar-derived a) volume extinction coefficient, and b) volume depolarization ratio, both with ceilometer-derived cloud bases shown in red, and c) radiosonde profiles of relative humidity (red) and lidar volume extinction coefficients (blue). The lidar is located at 365 m elevation while the radiosondes are launched approximately 5 km away at the airport near sea level, in generally drier conditions below 1 km.

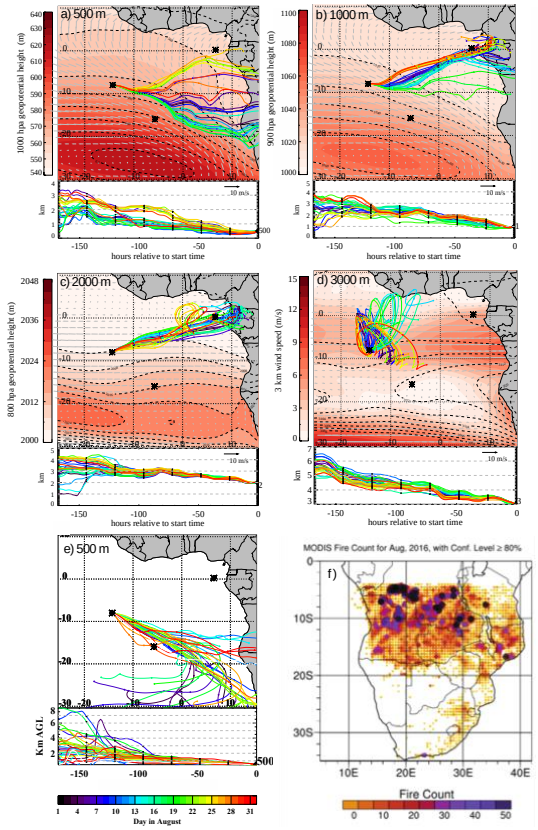

Fig. 12: 27-member ensemble HYSPLIT back trajectories initialized on 13 August 2016 12 UTC originating from Ascension Island at a) 500 m, b) 1 km, c) 2 km, and d) 3 km, driven by 0.5° NCEP GFS meteorology. The August-2016-mean ERA-Interim geopotential heights and vector winds are overlaid at a) 1000, b) 900, c) 800 and d) 700 hPa (dashed black contours, and as closed color contours on panels a)-c)). Panel d) indicates the 3 km wind speeds in closed color contours. e) One 500 m backtrajectory per day of August (12 UTC). f) Spatial distribution of MODIS-detected fires for August of 2016.

A further, separate, notable result is from the quality-controlled filter measurements, PSAP and the nephelometer, was that the single-scattering albedo increased systematically from August to October in both 2016 and 2017, with monthly-means of 0.78 +/- 0.02 (August), 0.81 +/-0.03 (September) and 0.83 +/-0.03 (October) at the green wavelength. The increase with time is consistent with Eck et al., (2013). What was initially surprising were the values themselves, which were lower than those previously reported within Leahy et al. (2012). Filter-based techniques such as the Particle Soot Absorption Photometer (PSAP), nephelometers and aethalometers estimate extinction from the change in light transmission through particle-imbibed filters. The Cavity Attenuated Phase Shift (CAPS)-SSA uses entirely different approach. It utilizes a unique optical design to simultaneously measure aerosol light extinction and scattering in the same sample volume. The LASIC SSA-CONSTRAINT study, a joint effort between Aerodyne and DOE ARM, brought a CAPS-SSA monitor to Ascension, with measurements made from August 4 to September 22, 2017. The CAPS-SSA measurements corroborate the PSAP absorption, and reported an average SSA value of 0.77 +-0.03 that supports the filter-based SSA measurements.

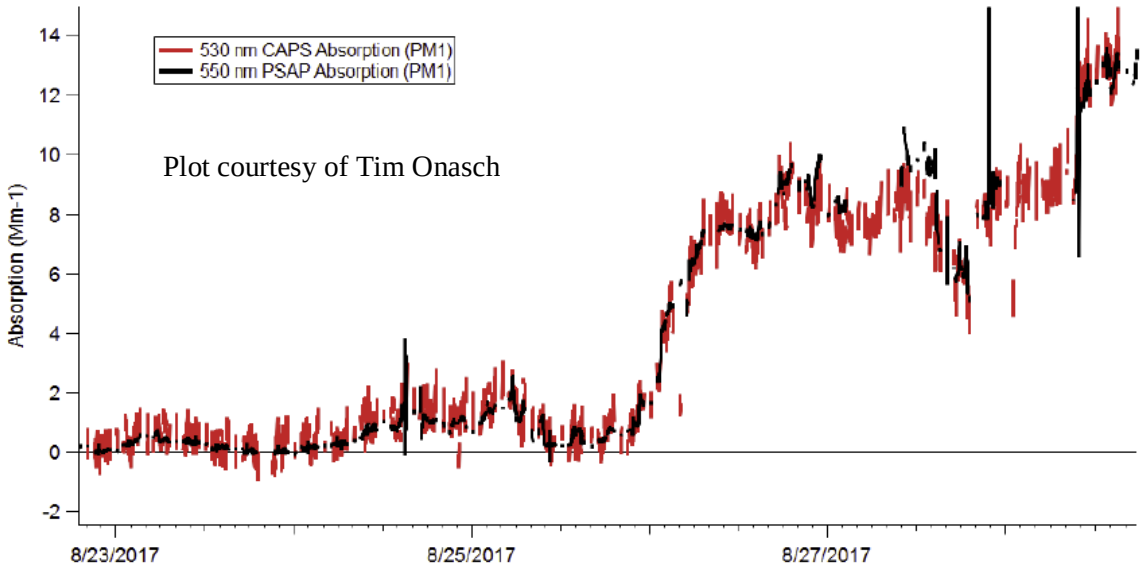

Instrument Issues: The W-band radars did not perform well, and little data are available from them. Doppler lidar data are not available for the first biomass-burning season in 2016.

3.Results

Please share results derived from the campaign. What are some further research opportunities? Include any images or data plots you would like to share, but this is not required.

Some initial results are shown in Zuidema et al. 2018 with its Figure 1 repeated here. The rBC mass concentrations already regularly exceed 10 ng m^{-3} by June. The variability is predominantly synoptic, with smokier and cleaner time periods able to alternate within a few days of each other. August is the smokiest month depicted, with a monthly-mean rBC mass concentration reaching almost 500 ng m^{-3}. The maximum rBC exceeded 1700 ng m^{-3} on 13 August, 2016, followed by another local maximum on 30

August. The peaks in the near-surface values are comparable to those measured closer to the African coast between 3-6 km altitude in September, 2016 by a NASA P-3 research plane. A strong subsequent decline in September occurs to much lower and even occasionally zero concentrations of black carbon. Nevertheless, even in November rBC mass values still exceeded 3 ng m^{-3} (the SP2 detection limit) 90% of the time, although overall the monthly-mean value was much lower at 32 ng m^{-3}. Few island sources exist for the black carbon, with the instrumentation located on the windward side of the island upwind from the site generator. Details of the aerosol light absorption variability with time track that of the rBC. Most of the aerosol can be activated into cloud condensation nuclei by supersaturations of 0.2%, more prominently so in June, indicating the aerosol's potential to modify clouds microphysically. A supersaturation of 0.2% is readily achieved in the marine environment (Wood et al., 2012). At 0.4% SS, all or nearly so of the condensation particles with diameters > 10 nm are activated. The variability in the carbon monoxide (CO) values indicates that clean background conditions representative of the atmosphere above the southern high-latitude ocean, determined when the CO is at the 0.06 ppm noise floor, can also occur, sometimes within only a few days of a heavy smoke event. Also evident is that the CO:particle count ratio increases over time; the CO:rBC ratio is also lower in June than in August-September, implying that either the aerosol in June is more aged (Heald et al., 2014) or stems from more actively flaming sources producing less CO compared to smoldering fires (Liu et al., 2013).

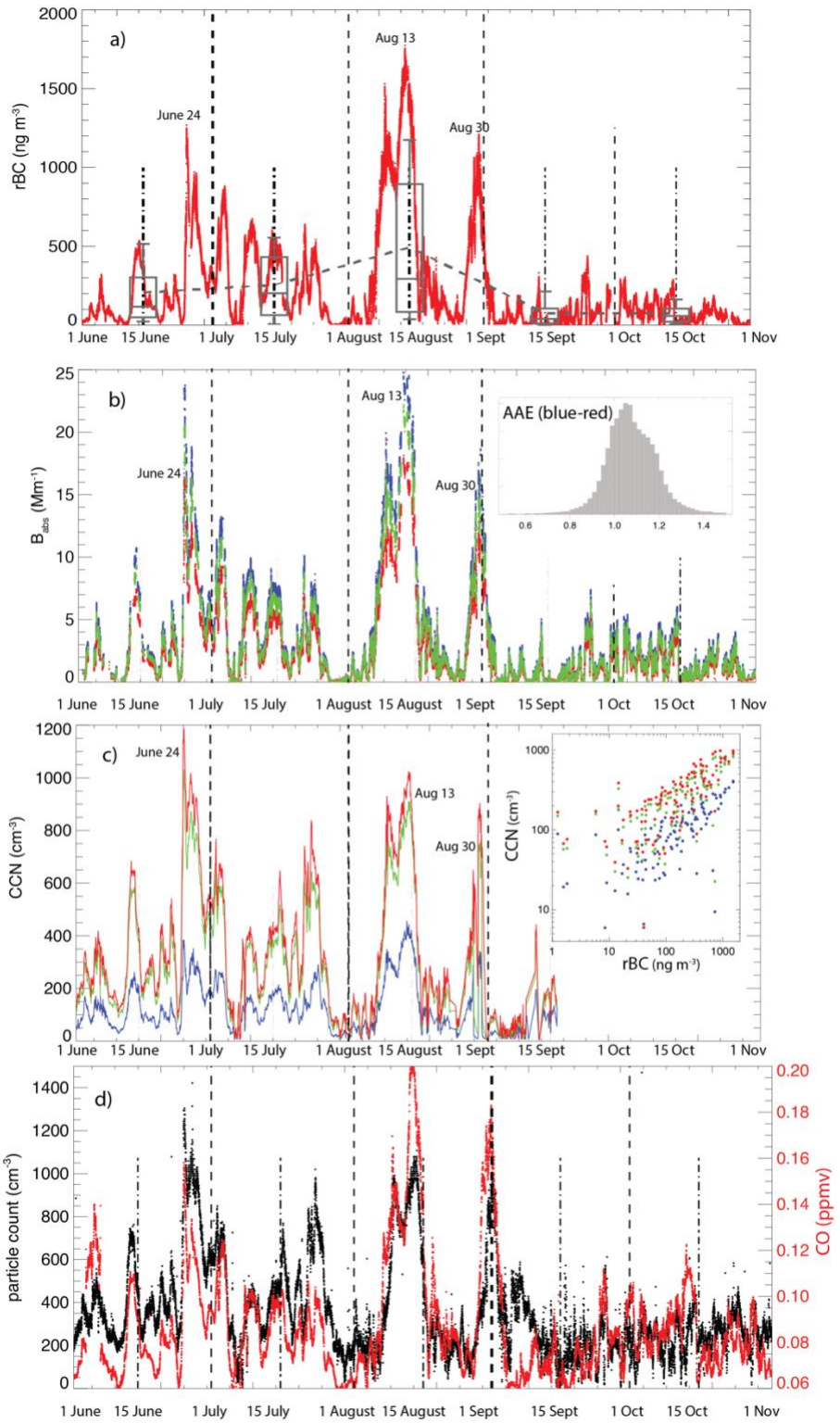

Fig. 13: 1 June - 31 October, 2016 time series of a) single-particle soot photometer (SP2)-derived refractory black carbon (rBC) mass concentrations. Monthly 10, 25, 50, 75, 90 percentiles are indicated, with a dotted line connecting monthly-mean values. b) Particle soot absorption photometer (PSAP) aerosol light absorption coefficients at three wavelengths (blue: 464 nm, green: 529 nm, red: 648 nm) as an average of the Virkkula1 (2010) and Ogren and Bond (2010) corrections. The inset indicates the relative frequency distribution of the blue-red absorption angstrom exponent, only calculated when the blue nephelometer-derived scattering > 10 Mm^{-1}. c) Cloud condensation concentrations (CCN) at 0.1%, 0.2% and 0.4% supersaturations (data from 15 September to 1 November are missing). Inset indicates daily-averaged CCN versus rBC mass concentrations. d) Condensation particle concentrations (black; minimum particle diameter of 10 nm) and carbon monoxide (red).

4.Public Outreach

The LASIC campaign is advertised through the URL https://www.arm.gov/research/campaigns/amf2016lasic. It has most recently been highlighted in the ARM March 2018 newsletter.

5.LASIC Publications

This section identifies any journal articles (published and/or submitted), presentations/meetings where results were presented, and references used in section 1 and 2.

Selected early findings mentioned under "2.0 Results" are now published in Zuidema et al., 2018. LASIC presentations have been made at the AGU annual meeting (2016 and 2017) by Allison Aiken, Sam Pennypacker and Rob Wood, and Jianhao Zhang, Rodrigo Delgadillo and Paquita Zuidema. The annual DOE ASR 2016 and 2017 meetings included LASIC-specific breakout sessions that included presentations by, in addition to those mentioned above, Yann Blanchard and Christine Chiu, Art Sedlacek, Stephen Springston, Connor Flynn, Tim Onasch, and Yang Fen.

References for Section 1:

Abel, S. J., J. M. Haywood, E. J. Highwood, J. Li, and P. R. Buseck, 2003: Evolution of biomass burning aerosol properties from an agricultural fire in southern Africa, *Geophys. Res. Lett.*, **30**(15), 1783, doi:10.1029/ 2003GL017342.

Abel, S., E. J. Highwood, J. Haywood and M. Stringer, 2005: The direct radiative effect of biomass burning aerosol over southern Africa, *Atmos. Chem. Phys.*, **5**, p. 1999-2018, doi: 1680-7324/acp/2005-5-1999.

Ackerman, A.S., O.B. Toon, D.E. Stevens, A.J. Heymsfield, V. Ramanathan, and E.J. Welton, 2000: Reduction of tropical cloudiness by soot. *Science,* **288**, 1042-1047

Adebiyi, A., P. Zuidema and S. Abel, 2015: The convolution of dynamics and moisture with the pres ence of shortwave absorbing aerosols over the southeast Atlantic. *J. Climate,* **28***,* p. 1997-2024*.* doi:10.1175/JCLI-D-14-00351.2.

Adebiyi, A. and P. Zuidema, 2016: The role of the southern African easterly jet in modifying the southeast Atlantic aerosol and cloud environments. *Q. J. R. Meteorol. Soc.,*

Akagi, S. K., J. S. Craven, J. W. Taylor, G. R. McMeeking, R. J. Yokelson, I. R. Burling, S. P. Urbanski, C. E. Wold, J. H. Seinfeld, H. Coe, M. J. Alvarado, and D. R. Weise, 2012: Evolution of trace gases and particles emitted by a chaparral fire in California, *Atmos. Chem. Phys.*, **12**, 1397-1421, doi:10.5194/acp-12-1397-2012.

Alvarado, M. J., C. R. Lonsdale, R. J. Yokelson, S. K. Akagi, H. Coe, J. S. Craven, E. V. Fischer, G. R. McMeeking, J. H. Seinfeld, T. Soni, J. W. Taylor, D. R. Weise, and C. E. Wold, 2014: Investigating the Links Between Ozone and Organic Aerosol Chemistry in a Biomass Burning Plume from a Prescribed Fire in California Chaparral, submitted to Atmos. Chem. Phys., manuscript number acp-2014-886.

Alvarado, M. J., and R. G. Prinn, 200: Formation of Ozone and Growth of Aerosols in Young Smoke Plumes from Biomass Burning, Part 1: Lagrangian Parcel Studies, J. Geophys. Res., 114, D09306, doi:10.1029/2008JD011144.

Andreae, M. O. and Rosenfeld, D., 2008: Aerosol-cloud- precipitation interactions. Part 1: The nature and sources of cloud-active aerosols, *Earth Sci. Rev.*, **89**, 13–41, doi:10.1016/j.earscirev.2008.03.001.

Bellouin N; Mann GW; Woodhouse MT; Johnson C; Carslaw KS; Dalvi M., 2013: Impact of the modal aerosol scheme GLOMAP-mode on aerosol forcing in the Hadley Centre Global Environmental Model. *Atmos. Chem. Phys.*, **13**, pp.3027-3044. doi: 10.5194/acp-13-3027-2013 ,

Bennartz, R., 2007:, Global assessment of marine boundary layer cloud droplet number concentration from satellite, *J. Geophys. Res*., **112**, D02201, doi:10.1029/2006JD007547

Bond, T. et al., 2013: Bounding the role of black carbon in the climate system: A scientific assessment. *J. Geophys. Res.*, **118**, p. 1-173. doi:10.1002/jgrd.50171.

Borque, P., P. Kollias and S. Giangrande, 2014: First Light Observations of Tracking Clouds Using Scan ning ARM Cloud Radars. Accepted to Journal of Applied Meteorology and Climatology

Boucher, O., D. Randall, P. Artaxo, C. Bretherton, G. Feingold, P. Forster, V.-M. Kerminen, Y. Kondo, H. Liao, U. Lohmann, P. Rasch, S. K. Satheesh, S. Sherwood, B. Stevens and X. Y. Zhang, 2013: Clouds and Aerosols. In: Climate Change 2013: The Physical Science Basis. Contribution of Working Group I to the Fifth Assessment Report of the Intergovernmental Panel on Climate Change [Stocker, T. F., D. Qin, G.-K. Plattner, M. Tignor, S. K. Allen, J. Boschung, A. Nauels, Y. Xia, V. Bex and P. M. Midgley (eds.)]. Cambridge University Press, Cambridge, United Kingdom and New York, NY, USA, in press

Brioude, J. et al., 2009: Biomass burning on marine stratocumulus clouds off of the Californian coast. *Atmos. Chem. Phys*., **9**, pp. 8841-8856. doi:10.5194/acp-10-8841-2010.

Brioude, J., et al., 2013: Top-down surface flux in the Los Angeles Basin using the inverse modeling technique: assessing anthropogenic NO_x and CO_2 and their impacts. *Atmos. Chem. Phys.*, **13**, 3661-3677, doi:10.5194/acp-13-3661-2013.

Chand, D.,R. Wood, T. L. Anderson, S. K. Satheesh and R. J. Charlso, 2009: Satellite-derived direct radiative effect of aerosols dependent on cloud cover. *Nature Geo*., doi:10.1038/ngeo0437

Chiu, C., A. Marshak, C.-H. Huang, T. Varnai, R. J. Hogan, D. Giles, B. Holben, E. O'Connor, Y. Knyazikhin and W. Wiscombe, 2012: Cloud droplet size and liquid water path retrievals from zenith radiance measurements: examples from the Atmospheric Radiation Measurement Pro gram and the Aerosol Robotic Network., *Atmos. Chem. Phys.*, **12**, doi:10.5194/acp-12-10313-2012.

Costantino, L. and Bre´on, F.-M., 2010: Analysis of aerosol-cloud interaction from multi-sensor satellite observations, *Geophys. Res. Lett.*, **37**, L11801, doi:10.1029/2009GL041828.

Costantino, L. and Bre´on, F.-M , 2013: Aerosol indirect effect on warm clouds over South-East Atlantic, from co-located MODIS and CALIPSO observations. *Atmos. Chem. Phys*., **13**, 69–88, doi: 10.5194/acp-13-69-2013

de Graaf, M., L. G. Tilstra, P. Wang, and P. Stammes, 2012:, Retrieval of the aerosol direct radiative effect over clouds from spaceborne spectrometry, *J. Geophys. Res*., **117**, D07207, doi:10.1029/2011JD017160.

de Graaf, M., N. Bellouin, L. G. Tilstra, J. Haywood, and P. Stammes, 2014: Aerosol direct radiative effect of smoke over clouds over the south- east Atlantic Ocean from 2006 to 2009, *Geophys. Res. Lett.*, **41**, 7723–7730, doi:10.1002/2014GL061103.

Duynkerke, P. G. and Coauthors, 2004: Observations and numerical simulations of the diurnal cycle of the EUROCS stratocumulus case. *Quart. J. Roy. Meteor. Soc.*, **130**, 3269–3296.

Eck, T. F., et al., 2013: A seasonal trend of single scattering albedo in southern African biomass-burning particles: Implications for satellite products and estimates of emissions for the world's largest biomass-burning source, *J. Geophys. Res. Atmos*., **118**, doi:10.1002/jgrd.50500.

Fang, M., R. J. Doviak, and Bruce A. Albrecht, 2012: Analytical Expressions for Doppler Spectra of Scat ter from Hydrometeors Observed with a Vertically Directed Radar Beam. *J. Atmos. Oceanic Technol.*, **29**, 500–509. doi: 10.1175/JTECH-D-11-00005.1

Feingold, G., H. Jiang, and J. Y. Harrington, 2005: On smoke suppression of clouds in Amazonia. *Geo phys. Res. Lett.*, **32**, No. 2, L02804, 10.1029/2004GL021369.

Fast, JD, WI Gustafson Jr., EG Chapman, RC Easter, JP Rishel, RA Zaveri, GA Grell, and MC Barth. 2011. The Aerosol Modeling Testbed: A Community Tool to Objectively Evaluate Aerosol Process Modules, Bulletin of the American Meteorological Society, **92**, 343-360. DOI:10.1175/2010BAMS2868.1

Feingold, G., and H. Siebert, 2009: Cloud-aerosol interactions from the micro to the cloud scale. Chapter 14 in Strungmann Forum report, vol. 2. Cambridge, MA: The MIT press.

Ghan, S. J., X. Liu, R. C. Easter, R. Zaveri, P. J. Rasch, J.-H. Yoon, B. Eaton, 2012: Toward a Minimal Representation of Aerosols in Climate Models: Comparative Decomposition of Aerosol Direct, Semidirect, and Indirect Radiative Forcing. *J. Climate*, **25**, 6461–6476.

Garstang, M., P. D. Tyson, R. Swap, M. Edwards, P. Kållberg, and J. A. Lindesay (1996), Horizontal and vertical transport of air over southern Africa, *J. Geophys. Res.*, **101**(D19), **23**,721–23,736,doi: 10.1029/ 95JD00844.

Granier et al., 2011: Evolution of anthropogenic and biomass burning emissions of air pollutants at global and regional scales during the 1980–2010 period. *Climatic Change*. **109**, p. 163-190. doi: 10.1007/s10584-011-0154-1

Hannay, C., D. L Williamson, J. J Hack, J. T Kiehl, J. G Olson, S. A Klein, C. S Bretherton, and M. Koehler ,2009: Evaluation of Forecasted Southeast Pacific Stratocumulus in the NCAR, GFDL and ECMWF Models. *J. Climate*, **22**, 2871-2889

Haywood, J. M., and K. P. Shine, 1995: The effect of anthropogenic sulfate and soot on the clear-sky planetary radiation budget, *Geophys. Res. Lett.*, **22**, 603–606.

Haywood, J. M., Osborne, S. R., Francis, P. N., Keil, A., Formenti, P., Andreae, M. O., and Kaye, P. H., 2003: The mean physical and optical properties of regional haze dominated by biomass burn- ing aerosol measured from the C-130 aircraft during SAFARI 2000, *J. Geophys. Res.*, **108**, 8473, doi: 10.1029/2002JD002226.

Haywood, J. M., S. R. Osborne, and S. J. Abel, 2004: The effect of overlying absorbing aerosol layers on remote sensing retrievals of cloud effective radius and cloud optical depth. *Q. J. R. Meteorol. Soc*., **130**, 779-800.

Hill, A., and S. Dobie, 2008: The impact of aerosols on non-precipitating stratocumulus. II: The semi-direct effect. *Q. J. R. M. S*., **134**, 155-165, doi:10.1002/qj.277.

Hobbs, P. V., P. Sinha, R. J. Yokelson, T. J. Christian, D. R. Blake, S. Gao, T. W. Kirchstetter, T. Novakov, and P. Pilewskie, 2003: Evolution of gases and particles from a savanna fire in South Africa, J. Geophys. Res., 108, 8485, doi:10.1029/2002JD002352, D13

Holben, B. N., et al., 2001: An emerging ground-based aerosol climatology: Aerosol optical depth from AERONET, *J. Geophys. Res*.,**106**(D11), 12,067–12,097, doi:10.1029/2001JD900014

Johnson, B., K. Shine and P. M. Forster, 2004: The semi-direct aerosol effect: Impact of absorbing aerosols on marine stratocumulus. *Q. J. R. Meteorol. Soc.*, **130**, pp. 1407-1422.

Johnson, B. T. (2005), Large-eddy simulations of the semidirect aerosol effect in shallow cumulus regimes, *J. Geophys. Res*., **110**, D14206, doi:10.1029/2004JD005601.

IPCC, 2013: Climate Change 2013: The Physical Science Basis. Contribution of Working Group I to the Fifth Assessment Report of the Intergovernmental Panel on Climate Change [Stocker, T. F., D. Qin, G.-K. Plattner, M. Tignor, S. K. Allen, J. Boschung, A. Nauels, Y. Xia, V. Bex and P. M. Midgley (eds.)]. *Cambridge University Press*, Cambridge, United Kingdom and New York, NY, USA, in press.

Kassianov, E. I., Flynn, C. J., Ackerman, T. P., and Barnard, J. C. (2007), Aerosol single-scattering albedo and asymmetry parameter from MFRSR observations during the ARM Aerosol IOP 2003, *Atmos. Chem. Phys*., **7,** 3341-3351, doi:10.5194/acp-7-3341-2007.

Kazil, J., H. Wang, G. Feingold, A.D. Clarke, J.R. Snider, *and* A. R.Bandy, 2011: Modeling chemical and aerosol processes in the transition from closed to open cells during VOCALS-REx, Atmos. Chem. Phys., 11, 7491–7514.

Klein, S.A. and Hartmann, D.L., 1993: The seasonal cycle of low stratiform clouds. *Journal of Climate*, **6**, pp. 1587–1606

Klein, S., 1997: Synoptic variability of low-cloud properties and meteorological parameters in the subtrop ical trade-wind boundary layer. *J. Climate*, **10**, p. 2018-

Kindel, B. C., P. Pilewskie, K. S. Schmidt, O. Coddington, and M. D. King, 2011:, Solar spectral absorption by marine stratus clouds: Measurements and modeling, *J. Geophys. Res*., **116,** D10203, doi: 10.1029/2010JD015071

Kinne, S., D. O'Donnel, P. Stier, S. Kloster, K. Zhang, H. Schmidt, S. Rast, M. Giorgetta, T. F. Eck, and B. Stevens, 2013:, MAC-v1: A new global aerosol climatology for climate studies, *J. Adv. Model. Earth Syst*., **5**, doi:10.1002/jame.20035

Koch, D., and A. D. Del Genio, 2010:, Black carbon semi-direct effects on cloud cover: Review and syn thesis, *Atmos. Chem. Phys*., **10**, 7685–7696

Koffi, B., et al., 2012:, Application of the CALIOP layer product to evaluate the vertical distribution of aerosols estimated by global models: AeroCom phase I results, *J. Geophys. Res.*, **117**, D10201, doi:10.1029/2011JD016858.

Kollias, P., J. Remillard, E. Luke and W. Szyrmer, 2011a: Cloud Radar Doppler Spectra in Drizzling Strati form Clouds. Part I: Forward Modeling and Remote Sensing Applications. *J. Geophys. Res.-At mospheres,* doi:10.1029/2010JD015237

Kollias P., W. Szyrmer, J. Remillard and E. Luke, 2011b: Cloud Radar Doppler Spectra in Drizzling Strati form Clouds. Part II: Observations and Microphysical Modeling of Drizzle Evolution. *J. Geophys. Res.-Atmospheres,* doi:10.1029/2010JD015238

Kollias, Pavlos, Nitin Bharadwaj, Kevin Widener, Ieng Jo, Karen Johnson, 2014a: Scanning ARM Cloud Radars. Part I: Operational Sampling Strategies. *J. Atmos. Oceanic Technol*., **31**, 569–582

Kollias, Pavlos, and Coauthors, 2014b: Scanning ARM Cloud Radars. Part II: Data Quality Control and Processing. *J. Atmos. Oceanic Technol*., **31**, 583–598.

Koren, I., Y. J. Kaufman, L. A. Remer, J. V. Martins, 2004: Measurement of the effect of Amazon smoke on inhibition of cloud formation. *Science* **303**: 1342 – 1345, doi: 10.1126/ S*cience*.1089424.

Lamer, K., Tatarevic, A., Jo, I., and Kollias, P.: Evaluation of gridded Scanning ARM Cloud Radar reflectiv ity observations and vertical Doppler velocity retrievals, *Atmos. Meas. Tech. Discuss*., **6**, 9579-9621, doi:10.5194/amtd-6-9579-2013, 2013

Lee, S.-S., G. Feingold, P. Y. Chuang, 2012: Effect of Aerosol on Cloud–Environment Interactions in Trade Cumulus. *J. Atmos. Sci*., **69**, 3607–3632.

Li, Zhujun, P. Zuidema, and P. Zhu, 2014: Simulated convective invigoration processes at trade-wind cu mulus cold pool boundaries. *J. Atmos. Sci.*, **71**, p. 2823-2841. doi:10.1175/JAS-D-13-0184.1

Lin, B., Patrick Minnis , Tai-Fang Fan , Yongxiang Hu & Wenbo Sun, 2010: Radiation characteristics of low and high clouds in different oceanic regions observed by CERES and MODIS, *International Journal of Remote Sensing*, **31**:24, 6473-6492, DOI: 10.1080/01431160903548005

Liu, X., et al., 2012: Toward a minimal representation of aerosol direct and indirect effects: Model descrip tion and evaluation, *Geosci. Model Devel.* doi:10.5194/gmd-5-709-2012.

Loeb, N. G., and G. L. Schuster, 2008: An observational study of the relationship between cloud, aerosol and meteorology in broken low-level cloud conditions, *J. Geophys. Res*., **113**, D14214, doi: 10.1029/2007JD009763

Ma, P.-L., Rasch, P. J., Wang, H., Zhang, K., Easter, R. C., Tilmes, S., Fast, J. D., Liu, X., Yoon, J.-H., Lamarque, J.-F., 2013. The Role of Circulation Features on Black Carbon Transport into the Arctic in the Community Atmosphere Model Version 5 (CAM5). *J. Geophys. Res.* **118(10)**, 4657-4669.

Mann, G. W., Carslaw, K. S., Spracklen, D. V., Ridley, D. A., Manktelow, P. T., Chipperfield, M. P., Picker ing, S. J., and Johnson, C. E., 2010: Description and evaluation of GLOMAP-mode: a modal global aerosol microphysics model for the UKCA composition-climate model, *Geosci. Model Dev.*, **3**, 519-551, doi:10.5194/gmd-3-519-2010.

Mann, J. A. L., J. C. Chiu, R. J. Hogan, E. J. O'Connor, T. S. L'Ecuyer, T. H. M. Stein, and A. Jefferson, 2013: Aerosol impacts on drizzle properties in warm clouds from ARM Mobile Facility maritime and continental deployments, *J. Geophys. Res. Atmos.*, **119**, doi: 10.1002/2013JD021339.

Mauger, G. S., and J. R. Norris, 2007: Meteorological bias in satellite estimates of aerosol-cloud relation ships, *Geophys. Res. Lett.*, **34**, L16824, doi:10.1029/2007GL029952.

McFarquhar, G. M., S. Platnick, L. D. Di Girolamo, H. Wang, G. Wind, and G. Zhao, 2004: Trade wind cumuli statistics in clean and polluted air over the Indian Ocean from in situ and remote sensing measurements. *Geophys. Res. Lett*., **31**, L21105, doi:10.1029/2004GL020412

McFarquhar, G. M., and H. Wang, 2006: Effects of aerosols on trade wind cumuli over the Indian Ocean: Model simulations. *Quart. J. Roy. Meteor. Soc.*, **132**, 821–843.

Mechoso, C., R. Wood, C. S. Bretherton, A. Clarke, H. Coe, C. Fairall, J. T. Farrar, G. Feingold, R. Gar reaud,C. Grados, J. McWilliams, S. de Szoeke, S. Yuter, P. Zuidema, 2014: Ocean-Cloud-At mosphere-Land Interactions in the Southeast Pacific: The VOCALS Program. *Bull. Amer. Meteor. Soc.*,**95**,p. 357-375. doi:10.1175/BAMS-D-11-00246.

Medeiros, B. D L Williamson, C Hannay, J Olson., 2012: *S*outheast Pacific stratocumulus in the Commu nity Atmosphere Model. *J. Climate*, **25**, 6175-6192

Meyer, K., S. Platnick, L. Oreopoulos, D. Lee, 2013: Estimating the direct radiative forcing of absorbing aerosols overlying marine boundary layer clouds in the southeast Atlantic using MODIS and CALIOP. *J. Geophys. Res*., DOI: 10.1002/jgrd.50449

Mlawer, E.J., P.D. Brown, S.A. Clough, L.C. Harrison, J.J. Michalsky, P.W. Kiedron, and T. Shippert, 2000: Comparison of spectral direct and diffuse solar irradiance measurements and calculations for cloud-free conditions, *Geophys. Res. Lett*., **27**, 2653-2656, 2000.

Moeng, C.-H., and Coauthors, 1996: Simulation of a stratocumulus- topped planetary boundary layer: Intercomparison among different numerical codes. *Bull. Amer. Meteor. Soc*., **77**, 261–278.

Moran, K., S. Pezoa, C. Fairall, C. Williams, T. Ayers, A. Brewer, S. de Szoeke, and V. Ghate, 2011: A motion-stabilitzed W-band radar for shipboard observations of marine boundary-layer clouds. *Boun. Layer Meteorol.* doi: 10.1007/s10546-011-9674-5.

Myrhe, G. et al., 2013: Radiative forcing of the direct aerosol effect from AeroCom Phase II simulations. *Atmos. Chem. Phys,* **13**, p. 1853-1877, doi:10.5194/acp-13/1853-2013.

Neggers, R. A. J., A. P. Siebesma, T. Heus, 2012: Continuous Single-Column Model Evaluation at a Permanent Meteorological Supersite. *Bull. Amer. Meteor. Soc.*, **93**, 1389–1400. doi: 10.1175/BAMS-D-11-00162.1

Noda, A. T., and M. Satoh, 2014: Intermodel variances of subtropical stratocumulus environments simu lated in CMIP5 models, *Geophys. Res. Lett*., **41**, 7754–7761, doi:10.1002/2014GL061812

Onasch, T.B., Massoli, P., Kebabian, P.L., Hills, F.B., Bacon, F.W., and Freedman, A. (2015). Single Scattering Albedo Monitor for Airborne Particulates. *Aerosol Sci. Technol.,* 49(4): 267-279. doi:10.1080/02786826.2015.1022248

Oktem, R., Prabhat, J. Lee, A. Thomas, P. Zuidema, D. M. Romps, 2014: Stereophotogrammetry of oceanic clouds. *J. Atmos. Ocean. Tech*., **31**, p.1482-1501. doi:10.1175/jtech-d-13-00224.

Painemal, D., and P. Zuidema, 2011: Assessment of MODIS cloud effective radius and optical thickness retrievals over the Southeast Pacific with VOCALS-REx in situ measurements, *J. Geophys. Res.*, **116**, D24206, doi:10.1029/2011JD016155.

Painemal D**.**, K-M Xu, A. Cheng, P. Minnis, and R. Palikonda (2014), Mean structure and diurnal cycle of Southeast Atlantic boundary layer clouds: Insights from satellite observations and multiscale modeling framework simulations, J. Climate (accepted)

Painemal D**.**, S. Kato, and P. Minnis (2014), Boundary layer regulation in the southeast Atlantic cloud mi crophysics during the biomass burning season as seen by the A-train satellite constellation, *J. Geophys. Res., 119, doi:10.1002/2014JD022182*

Petters, J. L., H. Jiang, G. Feingold, D. L. Rossiter, D. Khelif, L. C. Sloan, and P. Y. Chuang, 2013: A com parative study of the response of modeled non-drizzling stratocumulus to meteorological and aerosol perturbations. *Atmos. Chem. Phys*., **13**, 2507-2529, doi:10.5194/acp-13-2507-2013

Ramanathan , V., G. Carmichael, 2008: Global and regional climate changes due to black carbon, *Nature Geoscience*, **1**, 221-227.

Randles, C. and V. Ramaswamy, 2010: Direct and semi-direct impacts of absorbing biomass burning aerosol on the climate of southern Africa: A Geophysical Fluid Dynamics Laboratory GCM sensi tivity study. *Atmos. Chem. Phys.,* **10***,* p. 9819-9831, doi:10.5194/acp-10-9819-2010.

Redemann, J., Livingston, J., and Russel, P., 2010: A new method for deriving aerosol solar radiative forc ing and its first application within MILAGRO/INTEX-B, *Atmos. Chem. Phys*., **10**, 7829–7843, doi: 10.5194/acp- 10-7829-2010, 10, 2731-2767

Remer, L., 2009: Smoke above clouds. Nature Geo., **2**, p. 167-168.

Rémillard, Jasmine, Pavlos Kollias, Edward Luke, Robert Wood, 2012: Marine Boundary Layer Cloud Observations in the Azores. *J. Climate*, **25**, 7381–7398. doi: http://dx.doi.org/10.1175/JCLI-D-11-00610.1

Ross, K. E., S. J. Piketh, R. T. Bruintjes, R. P. Burger, R. J. Swap, and H. J. Annegarn, 2003:, Spatial and seasonal variations in CCN distribution and the aerosol-CCN relationship over Southern Africa,*J. Geophys. Res.*, **108,** 8481.

Russell, P. B., S. Kinne and R. Bergstrom, 1997: Aerosol climate effects: Local radiative forcing and column closure experiments, *J. Geophys. Res*., **102,** 9397-9407.

Sakaeda, N., R. Wood, and P. Rasch, 2011: Direct and semidirect aerosol effects of southern African biomass-burning aerosol, *J. Geophys. Res.,* **116**, D12205, doi:10.1029/2010JD015540.

Sandu, I., B. Stevens and R. Pincus, 2010: On the transitions in marine boundary layer clouds. *Atmos. Chem. Phys*., **10**, p. 2377-2391, doi:10.5194/acp-10-2377-2010.

Satheesh, S. K., O. Torres, L. A. Remer, S. S. Babu, V. Vinoj, T. F. Eck, R. G. Kleidman, and B. N. Holben (2009), Improved assessment of aerosol absorption using OMI-MODIS joint retrieval, J. Geophys. Res., 114, D05209, doi:10.1029/ 2008JD011024.

Schmidt, K. S., G. Feingold, P. Pilewskie, H. Jiang, O. Coddington, and M. Wendisch, 2009: Irradiance in polluted cumulus fields: Measured and modeled cloud-aerosol effects, *Geophys. Res. Lett.*, 36, L07804, doi:10.1029/2008GL036848.

Schmidt, K. S., Bierwirth, E., Coddington, O., Pilewskie, P., Wendisch, M., Bergstrom, R., Gore, W., Schulz, M., et al., 2006: Radiative forcing by aerosols as derived from the AeroCom present-day and pre-industrial simulations. *Atmospheric Chemistry and Physics*, **6**, 5225-5246.

Schulz, M., et al., 2006: Radiative forcing by aerosols as derived from the AeroCom present-day and pre-industrial simulations. *Atmospheric Chemistry and Physics*, **6**, 5225-5246.

Seidel, F. C. and Popp, C.2012: Critical surface albedo and its implications to aerosol remote sensing, *Atmos. Meas. Tech.*, **5**, 1653-1665, doi:10.5194/amt-5-1653-2012

Skamarock, W. C., and Coauthors, 2008: A description of the Advanced Research WRF, version 3. NCAR Tech. Note NCAR/TN-475+STR, 113 pp.

Soden, B. J., and G. A. Vecchi, 2011:, The vertical distribution of cloud feedback in coupled ocean-atmosphere models, *Geophys. Res. Lett*., **38**, L12704, doi: 10.1029/2011GL047632.

Sorooshian, A., G. Feingold, M. D. Lebsock, H. Jiang, and G. Stephens, 2009:, On the precipitation sus ceptibility of clouds to aerosol perturbations, *Geophys. Res. Lett*., **36**, L13803, doi: 10.1029/2009GL038993.

Sorooshian, A., G. Feingold, M. D. Lebsock, H. Jiang, and G. L. Stephens, 2010:, Deconstructing the pre cipitation susceptibility construct: Improving methodology for aerosol-cloud-precipitation studies, *J. Geophys. Res*., **115**, D17201,doi:10.1029/2009JD013426

Stevens, B., and Coauthors, 2005: Evaluation of large-eddy simulations via observations of nocturnal marine stratocumulus. *Mon. Wea. Rev.*, **133**, 1443–1462.

Stier P., N. A. J. Schutgens, N. Bellouin, H. Bian, O. Boucher, M. Chin, S. Ghan, N. Huneeus, S. Kinne, G. Lin, X. Ma, G. Myhre, J. E. Penner, C. A. Randles, B. Samset, M. Schulz, T. Takemura, F. Yu, H. Yu, and C. Zhou, 2013: Host model uncertainties in aerosol radiative forcing estimates: results from the AeroCom Prescribed intercomparison study *Atmos. Chem. Phys*., 13, 3245–3270, 2013 www.atmos-chem-phys.net/13/3245/2013/doi:10.5194/acp-13-3245-2013

Swap, R. et al., 2003: Africa burning: A thematic analysis of the Southern African Regional Science Initia tive (SAFARI 2000). *J. Geophys. Res.*, **108**, doi:10.1029/2003JD003747.

Terai, C. R., R. Wood, D. C. Leon, and P. Zuidema (2012), Does precipitation susceptibility vary with in creasing cloud thickness in marine stratocumulus?, *Atmos. Chem. Phys*., *12*, 4567–4583.

Tridon, Frédéric, Alessandro Battaglia, Pavlos Kollias, Edward Luke, Christopher R. Williams,2013: Signal Postprocessing and Reflectivity Calibration of the Atmospheric Radiation Measurement Program 915-MHz Wind Profilers. J. Atmos. Oceanic Technol., **30**, 1038–1054.
doi: http://dx.doi.org/10.1175/JTECH-D-12-00146.1

Turner, D.D., and U. Loehnert, 2014: Information content and uncertainties in thermodynamic profiles and liquid cloud properties retrieved from the ground-based Atmospheric Emitted Radiance Interfer ometer (AERI). *J. Appl. Meteor. Clim.*, 53, 752-771, doi:10.1175/JAMC-D-13-0126.1

Twomey, S., 1977: The influence of pollution on the shortwave albedo of clouds, *J. Atmos. Sci*., **34**, 1149– 1152.

Vakkari, V., et al., 2014: Rapid changes in biomass burning aerosols by atmospheric oxidation, *Geophys. Res. Lett.*, **41**, 2644–2651, doi:10.1002/ 2014GL059396.

van der Werf, G. R., Randerson, J. T., Giglio, L., Collatz, G. J., Kasibhatla, P. S., and Arellano Jr., A. F., 2006: Interannual variability in global biomass burning emissions from 1997 to 2004, *Atmos. Chem. Phys*., **6**, 3423–3441, 2006, 3648,

van der Werf, et al., 2010: Global fire emissions and the contribution of deforestation, savanna, forest, agricultural and peat fires (1997-2009), *Atmos. Chem. Phys*., **10**, 11707–11735, 2010, doi: 10.5194/acp-10-11707-2010

Voigt, B. Stevens, S. Bony, O. Boucher, 2013 : Easy Aerosol - a modeling framework to study robustness and sources of uncertainties in aerosol-induced changes of the large-scale atmospheric circula

tion. available through wcrp-climate.org/index.php/gc-clouds-circulation- activities/ gc4-clouds-initiatives/368-gc-clouds-inititative3-easy-aerosol

Wang, H., and G. Feingold, 2009a: Modeling mesoscale cellular structures and drizzle in marine stra tocumulus. Part I: Impact of drizzle on the formation and evolution of open cells. *J. Atmos. Sci*., **66**, 3237–3256.

Wang, H., and G. Feingold, 2009b: Modeling mesoscale cellular structures and drizzle in marine stra tocumulus. Part II: The microphysics and dynamics of the boundary region between open and closed cells. *J. Atmos. Sci.*, **66,** 3257–3275.

Wang, H., W. C. Skamarock, and G. Feingold, 2009: Evaluation of scalar advection schemes in the Ad vanced Research WRF model using large-eddy simulations of aerosol–cloud interactions. *Mon. Wea. Rev*., **137**, 2547–2558.

Wang H, G Feingold, R Wood, and J Kazil. 2010: Modelling microphysical and meteorological controls on precipitation and cloud cellular structures in Southeast Pacific stratocumulus. *Atmos. Chem. Phys* 10(13):6347-6362. doi:10.5194/acp-10-6347-2010

Wang, H., RC Easter, Jr, PJ Rasch, M Wang, X Liu, SJ Ghan, Y Qian, JH Yoon, PL Ma, and V Vinoj, 2013: Sensitivity of remote aerosol distributions to representation of cloud-aerosol interactions in a global climate model. *Geosci. Model Devel. 6,* 765–782.

Wang, H., P. J. Rasch, R. C. Easter, B. Singh, R. Zhang, P.-L. Ma, Y. Qian, S. J. Ghan, and N. Beagley. 2014:, Using an explicit emission tagging method in global modeling of source-receptor relation ships for black carbon in the Arctic: Variations, sources, and transport pathways, J. Geophys. Res. Atmos., 119, doi:10.1002/2014JD022297

Wang, M., et al. (2012), Constraining cloud lifetime effects of aerosols using A-Train satellite observations, *Geophys. Res. Lett*., *39*, L15709, doi:10.1029/2012GL052204.

Waquet, F., F. Peers, F. Ducos, P. Goloub, S. Platnick, J. Riedi, D. Tanre and F. Thieuleux, 2013: Global analysis of aerosol properties above clouds. *Geophys. Res. Lett.*, doi:10.1002/2013GL057482.

Welton, E. J., J. R. Campbell, J. D. Spinhirne, and V. S. Scott, 2001: Global monitoring of clouds and aerosols using a network of micro-pulse lidar systems, in Lidar Remote Sensing for Industry and Environmental Monitoring, U. N. Singh, T. Itabe, N. Sugimoto, (eds.), Proc. SPIE, 4153, 151-158

Wen, G., A. Marshak, R. F. Cahalan, L. A. Remer, and R. G. Kleidman, 2007:, 3-D aerosol-cloud radia tive interaction observed in collocated MODIS and ASTER images of cumulus cloud fields, *J. Geophys. Res*., **112**, D13204, doi:10.1029/2006JD008267

Wilcox, 2010: Stratocumulus cloud thickening beneath layers of absorbing smoke aerosol. *Atmos. Chem. Phys.,* **10,** pp. 11769-11777.

Wilcox, E. M.,2012: Direct and semi-direct radiative forcing of smoke aerosols over clouds, *Atmos. Chem. Phys.*, **12,** 139-149, doi:10.5194/acp-12-139-2012, 2012

Wood, R. ,2007: Cancellation of aerosol indirect effects in marine stratocumulus through cloud thinning, *J. Atmos. Sci.,* **64**, 2657–2669, doi:10.1175/JAS3942.1

Wood, R., et al., revised: Clouds, Aerosol, and Preciptation in the Marine Boundary Layer: An ARM Mobile Facility Deployment, *Bull. Amer. Meteor. Soc.*

Wyant, M. C., and Coauthors, 2007: A single-column model intercomparison of a heavily drizzling stra tocumulus-topped boundary layer. *J. Geophys. Res*., **112**, D24204, doi:10.1029/ 2007JD008536.

Yang, Q., W. I. Gustafson Jr., J. D. Fast, H. Wang, R. C. Easter, H. Morrison, Y.-N. Lee, E. G. Chapman, S. N. Spak, *and* M. A. Mena-Carrasco, 2011: Assessing regional scale predictions of aerosols, marine stratocumulus, and their interactions during VOCALS-REx using WRF-Chem, *Atmos. Chem. Phys*., **11**, 11,951–11,975.

Yang, Q., W. I. Gustafson Jr., J. D. Fast, H. Wang, R. C. Easter, M. Wang, S. J. Ghan, L. K. Berg, L. R. Leung, *and* H. Morrison, 2012: Impact of natural and anthropogenic aerosols on stratocumulus and precipitation in the Southeast Pacific: A regional modelling study using WRF-Chem, *Atmos. Chem. Phys*., **12**, 14,623–14,667.

Zhang, J. and J. S. Reid, 2010: A decadal regional and global trend analysis of the aerosol optical depth using data-assimilation grade over-water MODIS and Level 2 MISR aerosol products. *Atmos. Chem. Phys*., **10**, 10949–10963, doi:10.5194/acp-10-10949-2010

Zhang, M. H., and J. L. Lin, 1997: Constrained variational analysis of sounding data bases on column-integrated budgets of mass, heat, moisture, and momentum: Approach and application to ARM measurements, *J. Atmos. Sci.*, **54**, 1503-1524.

Zhang, M. H., J. L. Lin, R. T. Cederwall, J. J. Yio, and S. C. Xie, 2001: Objective Analysis of ARM IOP Data: Method and Sensitivity, *Mon. Weather Rev*., **129(2)**, 295-311, doi:10.1175/1520-0493(2001)129

Zhu, P., and Coauthors, 2005: Intercomparison and interpretation of single-column model simulations of a nocturnal stratocumulus- topped marine boundary layer. *Mon. Wea. Rev*., **133**, 2741– 2758

Zuidema, P., H. Xue, and G. Feingold, 2008: Shortwave radiative impacts from aerosol effects on shallow marine cumuli. *J. Atmos. Sci.*, **65**, pp. 1979-1990.

Zuidema, P., Z. Li, R. Hill, L. Bariteau, B. Rilling, C. Fairall, W. A. Brewer, B. Albrecht and J. Hare, 2012: On trade-wind cumulus cold pools. *J. Atmos. Sci.*, **69**, pp. 258-277, doi: 10.1175/jas-d-11-0143.1

5.1Journal Articles/Manuscripts

P. Zuidema and A. Sedlacek and C. Flynn and S. Springston and R. Delgadillo and J. Zhang and A. Aiken and P. Muradyan, 2018: The Ascension Island boundary layer in the remote southeast Atlantic is often smoky. *Geophys. Res. Lett.*, doi:10.1002/2017GL076926

5.2Meeting Abstracts/Presentations/Posters

From the DOE ASR 2018 LASIC-focused breakout session:

1. Allison Aiken - ambient aerosols in both smoky and reference conditions
2. Art Sedlacek - refractory black carbon
3. Tim Onasch - LASIC CAPS measurements
4. Connor Flynn - perspectives on filter-based derived SSA values

5. Yan Feng - Meteorological Influences on Biomass Burning Aerosol Long-range Transport: Observations vs CAM5 Simulations
6. Yann Blanchard - Cloud properties from zenith-pointing and scanning cloud radars: statistics and implications
7. Ewan O'Connor - inferences on turbulence from the Doppler lidar
8. Rob Wood: ultra-clean conditions at Ascension
9. Laura Riihimaki - update on VAP status
10. Tak Yamaguchi - perspectives on absorbing-aerosol-cloud interactions gained from recent modeling studies
11. Xiaohong Liu - WRF-Chem simulations of the southeast Atlantic
12. Zuidema/Saide - a community model-observational intercomparison project+assessment of WRF-CAM5 simulations using LASIC data

2.0 References

Please include a list of references used throughout this final campaign report

See section 4.0